MATERIALS SCIENCE

Motion lubrication suppressed mechanical activation via hydrated fibrous gene patch for tendon healing

Lei Xiang†, Jing Liang†, Zhen Wang, Feng Lin, Yaping Zhuang, Qimanguli Saiding, Fei Wang, Lianfu Deng, Wenguo Cui*

Mechanical activation of fibroblasts, caused by friction and transforming growth factor–β1 recognition, is one of the main causes of tissue adhesions. In this study, we developed a lubricated gene-hydrogel patch, which provides both a motion lubrication microenvironment and gene therapy. The patch's outer layer is composed of polyethylene glycol polyester hydrogel. The hydrogel forms hydrogen bonds with water molecules to create the motion lubrication layer, and it also serves as a gene delivery library for long-term gene silencing. Under the motion lubricated microenvironment, extracellular signal–regulated kinase–small interfering RNA can silence fibroblasts and enhance the blocking effect against fibroblast activation. In vitro, the proposed patch effectively inhibits fibroblast activation and reduces the coefficient of friction. In vivo, this patch reduces the expression of vimentin and α–smooth muscle actin in fibroblasts. Therefore, the lubricated gene-hydrogel patch can inhibit the mechanical activation of fibroblasts to promote tendon healing.

INTRODUCTION

Motion and lubrication are not only essential for organs to perform physiological functions but also directly affect cell signal transmission and disease progression (*1*, *2*). For instance, microdamage and envelope formation caused by direct friction between the injured area and the surrounding tissue or implants often lead to suboptimal tissue healing and exacerbate tissue adhesions (*3*, *4*). Annually, the cost of medical care for ligament and joint entrapment caused by tissue adhesions exceeds $10 billion (*5*, *6*). In the early stages of soft tissue injury, fibroblast activation caused by mechanical stimulation and inflammatory factors initiates the process of tissue adhesion and fibrosis (*7*, *8*). These activated cells attach to the injured area by recognizing exposed calmodulin, integrins, and hydrophobic binding thresholds, resulting in the loss of mobility (*9*–*11*). In addition, soft tissue injuries are often accompanied by damage to the surrounding mucosa and synovial structures. The loss of lubrication protection around the injury area causes difficulty in movement and aseptic inflammation, and it also accelerates the process of fibroblast mechanical activation, giving rise to a vicious cycle of "adhesion-release and re-adhesion" during soft tissue repair (*12*). Therefore, it is essential to restore the lubricating environment around the soft tissue while inhibiting the mechanical activation of fibroblasts to prevent tissue adhesions.

When exposed to mechanical stimulation such as friction, fibroblasts mechanically activate transforming growth factor–β1 (TGF-β1) that is latent in the extracellular matrix, leading to tissue adhesion and fibrosis (*13*). Now, drugs such as nonsteroidal anti-inflammatory drugs (NSAIDs), rapamycin, and quercetin are often delivered to the body by systemic or topical administration to address the biological mechanisms of tissue adhesion (*14*, *15*). Although these drugs can alleviate tissue adhesions by reducing inflammation levels, inducing apoptosis, and inhibiting oxidative stress, they cannot effectively inhibit fibroblast mechanical activation caused by the loss of lubrication protection. In situ gene silencing technology, which achieves mRNA sequence-specific degradation by delivering small interfering RNA (siRNA) to target cells, has been proven to be an effective advanced therapy (*16*–*18*). Previous studies have demonstrated that the TGF-β1–extracellular signal–regulated kinase 2 (ERK2) signaling axis plays a vital role in fibroblast proliferation. Silencing ERK2 and its downstream gene expression is a potential therapeutic method to prevent fibroblast activation and proliferation (*19*, *20*). Therefore, targeted silencing of the ERK2 gene in fibroblasts by constructing suitable gene vectors is the key to addressing the biological factors of adhesion. However, gene silencing alone cannot reduce the mechanical stimulation of fibroblasts, so it allows for suboptimal wound healing and recurrence of adhesions. Now, antiadhesive films such as Intergel and Oxiplex are commonly used in clinical practice. However, their nonlubricated surface and the potential Arg-Gly-Asp sequence enhance the mechanical stimulation of fibroblasts and lead to secondary adhesions (*21*–*26*). Therefore, it is urgent to develop a treatment to inhibit fibroblast activation and tissue adhesion by rebuilding a motion lubrication environment and silencing key gene expression.

Tendon adhesions are a common sports medicine condition caused by fibroblast mechanical activation under an unlubricated environment (*27*–*29*). The lack of a motion lubricated protection layer increases the coefficient of friction during tendon movement, which leads to difficulties in tendon movement and enhances fibroblast mechanical activation (*30*). In the absence of motor lubrication, the mechanical activation of fibroblasts around the tendon directly leads to increased levels of fibrosis and vascularization, resulting in the loss of the original physiological structure of the tendon. It has been demonstrated that a stable motion lubrication layer secreted by the tendon sheath and other tendon accessory tissues is a vital factor in maintaining the integrity of the tendon during frequent friction (*31*–*34*). Under physiological conditions, the presence of a hydrated lubricating layer on the tendon surface

Department of Orthopedics, Shanghai Key Laboratory for Prevention and Treatment of Bone and Joint Diseases, Shanghai Institute of Traumatology and Orthopedics, Ruijin Hospital, Shanghai Jiao Tong University School of Medicine, 197 Ruijin 2nd Road, Shanghai 200025, P.R. China.
*Corresponding author. Email: wgcui80@hotmail.com
†These authors contributed equally to this work.

can effectively prevent the mutual recognition of integrin protein and hydrophobic structural domains between the cell and the extracellular matrix, thus blocking the process of mechanical activation and improving tendon healing from the vicious cycle of adhesion–release–re-adhesion to a virtuous cycle of lubrication-antiadhesion-lubrication (*35*). Inspired by this, targeting the key biological and physical factors influencing the mechanical activation of fibroblasts, the construction of a hydrated lubricating bionic tendon sheath combined with gene silencing therapy has the potential to break the vicious cycle of tendon healing.

Combining motion lubrication with gene silencing to synergistically block the mechanical activation process from upstream and downstream is the key to promoting adhesion-free tendon healing. In this study, we constructed a lubricated gene-hydrogel patch, which can reshape tendon lubrication protection and synergistically block fibroblast mechanical activation to prevent tendon adhesions in terms of both molecular biological mechanisms and the physical friction microenvironment (Fig. 1). On the basis of the therapeutic idea of silencing the causative gene and shielding the adhesion site, a lubricated gene-hydrogel patch with a two-layer structure was constructed by combining polyethylene glycol (PEG)–based polyester hydrogel with electrostatic spinning technology. The ether bonds of PEG polyester hydrogel can form hydrogen bonds with water molecules to establish a stable motion lubrication and anti-cell adhesion domain, thereby reducing the coefficient of friction and avoiding the mechanical activation of fibroblasts. In addition, the hydrophobic poly(lactic-*co*-glycolic acid) (PLGA) fiber membrane on the inner side can effectively prevent hydrophilic ERK2-siRNA from being released to the injured site of the tendon. The temperature sensitivity of the PEG-based polyester hydrogel can effectively protect the biological activity of the loaded ERK2-siRNA and efficiently silence the intracellular ERK2 gene at the early stage of inflammation. In vitro, the lubricated gene-hydrogel patch specifically silences ERK2 gene expression, thus reducing the motion coefficient of friction and preventing cell mechanical activation. In vivo, under motion lubrication, the lubricated gene-hydrogel patch effectively reduces the level of tissue adhesion, fibrosis, and vascularization caused by the mechanical activation of fibroblasts (Fig. 2).

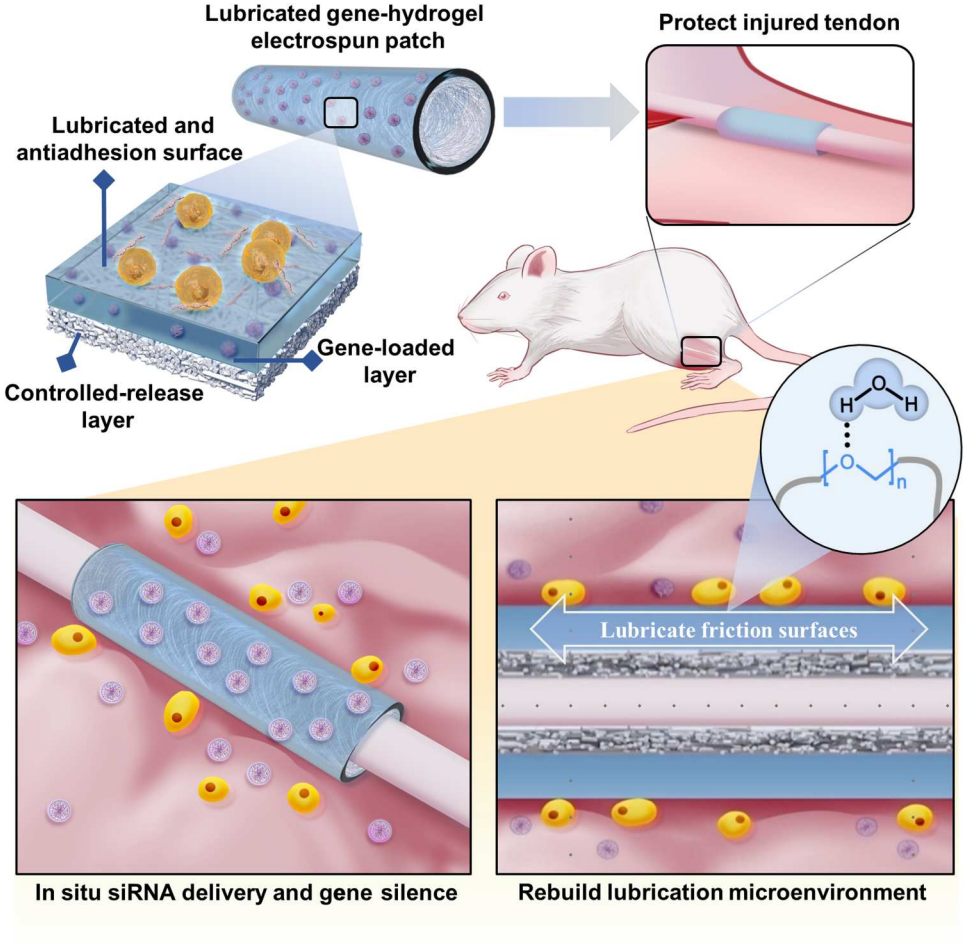

Fig. 1. The graphic abstract of lubricated gene patch for tendon healing. To prevent the tissue adhesion caused by the mechanical activation of fibroblasts, the lubricated gene-hydrogel patch was designed. On the basis of the affinity of PEG for H_2O, the lubricated layer can efficiently reduce frictional stress to inhibit the mechanical activation of fibroblasts. Combined with unidirectional gene silencing, the patch can efficiently prevent the activation and proliferation of fibroblasts to improve tendon healing.

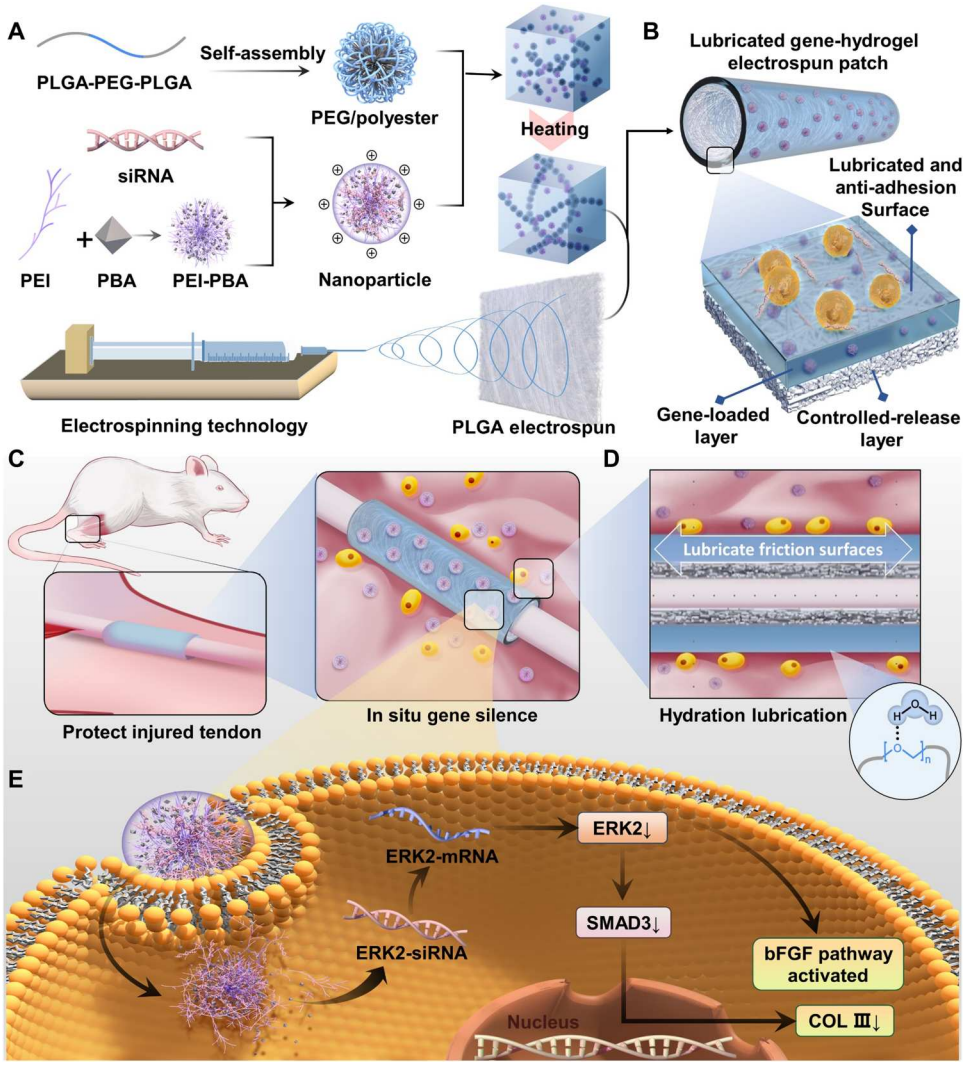

Fig. 2. Overview of the proposed lubricated gene-hydrogel patch. (**A**) Schematic representation of the synthesis of PEI-PBA gene nanocomplexes, temperature-sensitive PEG polyesters, and the preparation of PLGA electrospun membrane. (**B**) Schematic representation of the fabrication of the lubricated gene-hydrogel patch and its functional area division. (**C**) Lubricated gene-hydrogel patch can wrap and protect the injured tendon in situ. (**D**) PEG polyester hydrogel outer layer forms a stable lubricating layer around the tendon for reconstructing the lubrication microenvironment. (**E**) Double-layer structure enables the unidirectional release of gene nanoparticles loaded in the hydrogel layer to achieve targeted ERK2 and downstream gene silencing. bFGF, basic fibroblast growth factor.

RESULTS

Construction of PEI-PBA gene nanocomplexes

Overexpression of the ERK2 gene is not only the key to fibroblast overproliferation but also the key gene mediating TGF-β1 mechanical activation signaling in fibroblasts, which leads to peritendinous adhesions. Therefore, achieving efficient and stable silencing of ERK2 gene expression in fibroblasts is essential to blocking the mechanical activation of fibroblasts (*19*, *20*). Although a lentivirus-based siRNA delivery system can effectively regulate the gene expression of cells, its potentially poor biosafety restricts its further utilization in vivo (*36*–*38*). Gene delivery vectors represented by polycations are used for intracellular gene delivery through charge interactions (*39*, *40*). Although cationic gene delivery vectors represented by polyethyleneimine (PEI) have extremely high transfection efficiency, their cytotoxicity limits their further application in organisms (*41*, *42*). As shown in Fig. 3A, to obtain efficient and safe gene carriers, we solved the cytotoxicity problem caused by the high positively charged PEI by grafting the negatively charged phenylboronic acid (PBA) group onto the PEI branched chain through a simple synthetic method. In addition, PBA can target the recognition of glycoproteins and glycols on the cell membrane, which can effectively improve transfection efficiency (*43*).

We determined the specific structure of the synthesized PEI-PBA based on its ^{1}H nuclear magnetic resonance (NMR) spectrum. Peaks in the range of 6.75 to 7.75 parts per million (ppm) were the characteristic peaks on the benzene ring of PBA, and peaks in the range of 3.5 to 2.5 ppm were attributed to the characteristic peaks of methylene on PEI-25000, proving that our synthetic method can prepare PEI-PBA easily and efficiently (Fig. 3B). The surface potential and particle size of the cationic carriers directly affect the gene transfection efficiency, and we further characterized the PEI-PBA polycationic carriers. We found that the mass ratio *M*

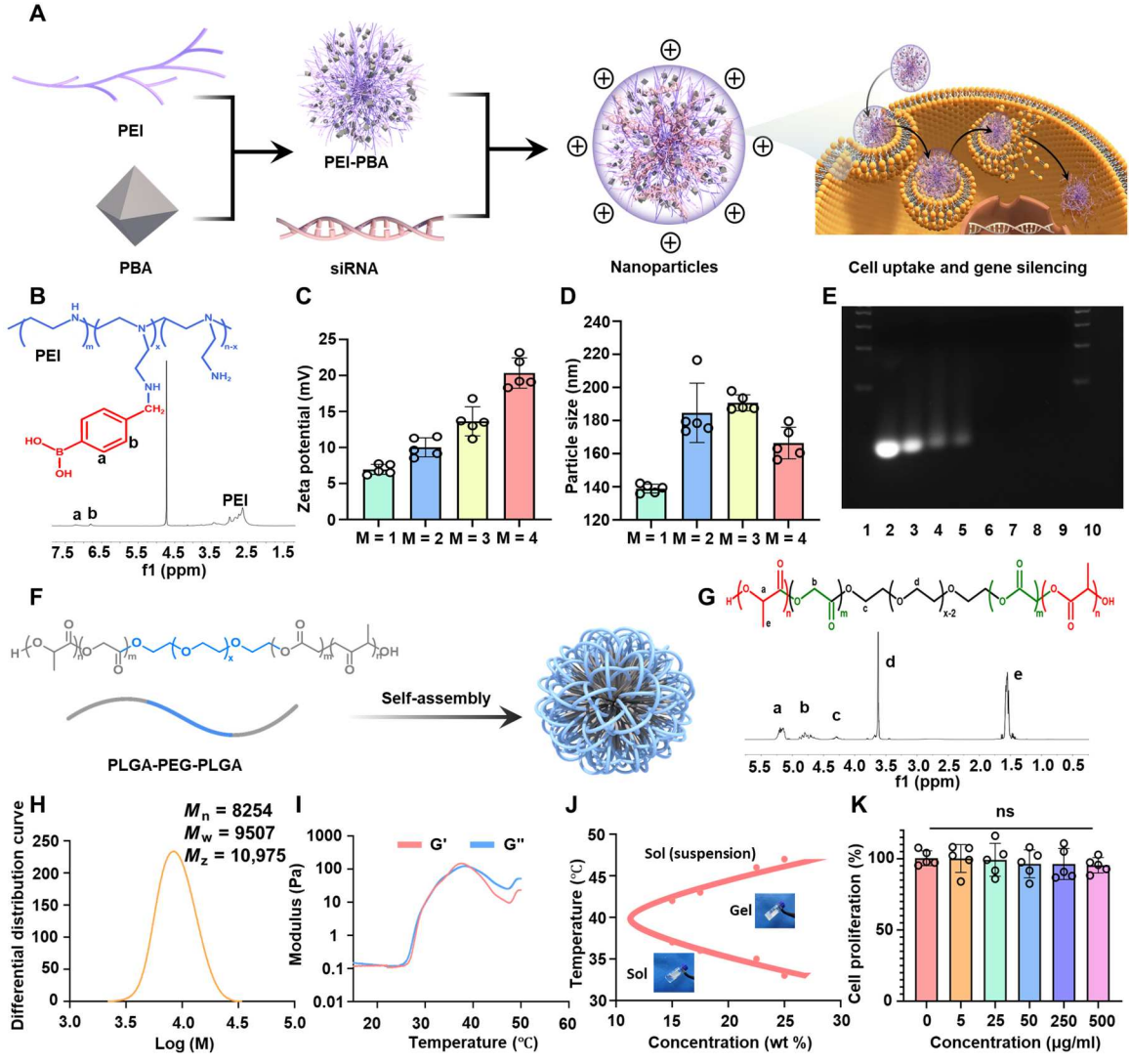

Fig. 3. Characterization of PEI-PBA gene nanocomplex and PEG polyesters. (**A**) Synthesis and gene delivery mechanism of PEI-PBA gene nanocomplexes. (**B**) ^{1}H NMR spectra of PEI-PBA. (**C**) Zeta potential of PEI-PBA gene nanocomplexes. (**D**) Particle size of PEI-PBA gene nanocomplexes. (**E**) Characterization of PEI-PBA gene nanocomplexes using 3% agarose gel electrophoresis. Lanes 1 and 10 represent maker. Lanes 2 to 9 represent M = 0.0625, M = 0.125, M = 0.25, M = 0.5, M = 1, M = 2, M = 3, and M = 4 PEI-PBA@ERK2-siRNA in that order. (**F**) Chemical structure of PEG polyesters and their self-assembly processes. (**G**) ^{1}H NMR spectra of PEG polyesters. (**H**) Gel permeation chromatogram traces of PEG polyester. (**I**) Storage modulus (G') and loss modulus (G'') of PEG polyesters. Heating rates: 0.5°C/min and oscillatory frequency: 10 rad/s. The polymer concentration was 25 wt %. (**J**) Phase diagram of the PEG polyester aqueous solutions was determined by the test tube inverting method. (**K**) Biocompatibility of PEG was determined by the CCK-8 kit (n = 5). M_n, number-average molecular weight; M_w, weight-average molecular weight; M_z, z-average molecular weight.

[$M = M_{(\text{PEI-PBA})}/M_{(\text{siRNA})}$] directly affects the particle size and surface potential of the formed gene nanoparticles. As shown in Fig. 3 (C and D), the surface potential of gene nanoparticles increased from 5.95 ± 0.62 mV to 17.62 ± 1.88 mV ($P < 0.05$) when the mass ratio of the gene nanoparticles increased (M = 1, 2, 3, and 4). Compared to M = 3, the particle size of gene nanoparticles at M = 4 decreased from 190.74 ± 4.27 nm to 166.42 ± 8.54 nm ($P < 0.05$), which may have been due to the increase of positive charge compressing the negatively charged siRNA and making the nanoparticles more compact. We further investigated the binding ability of PEI-PBA with siRNA by agarose gel electrophoresis experiments. As shown in Fig. 3E, the binding ability of PEI-PBA with siRNA was proportional to the mass of PEI-PBA. When $M \geq 1$, PEI-PBA could effectively bind to siRNA and prevent the escape of siRNA during electrophoresis, proving that the excellent binding ability of PEI-PBA to siRNA can ensure the structural stability of gene nanoparticles in the transfection process.

Construction of temperature-sensitive PEG polyesters

Tissue adhesion is a process in which cells interact with nearby cells through specialized molecules. The mechanical activation of fibroblasts requires mutual recognition between cells and TGF-β1 latent in the extracellular matrix, which can be inhibited if the mutual recognition between cells and the extracellular matrix is blocked (*44*).

Therefore, we envisioned PEG as a potential lubricant and anti-cell adhesion material (*45*). Accordingly, we obtained PEG polyesters through ring-opening polymerization of glycolide (GA) and D,L-lactide (LA) monomers using PEG-1500 as the initiator and stannous octanoate [$Sn(Oct)_2$] as the catalyst. The synthesis of PEG polyesters is illustrated in Materials and Methods. As shown in Fig. 3F, the PEG polyesters can self-assemble into nanoparticles with PLGA as the hydrophobic core and PEG as the hydrophilic outer layer at 36° to 37°C. Figure 3G shows the chemical structural formula of PEG polyester and its ^{1}H NMR spectrum. Figure 3H shows the gel permeation chromatogram (GPC) data of PEG polyester, and table S1 summarizes the molecular parameters of PEG polyester, indicating that we successfully synthesized the desired polymer. As shown in fig. S1, 25 weight % (wt %) aqueous solutions of PEG polyester can flow freely at/or below room temperature, and the sol-gel phase transition occurs with increasing temperature. We investigated the phase transition behavior of polymer solutions with increasing temperature by strain-controlled rheometry. Usually, the intersection temperature of the modulus of elasticity (G') and the modulus of loss (G'') is defined as the sol-gel transition temperature. When G' is higher than G', the system has transformed into a gel. As shown in Fig. 3I, the phase transition temperature of PEG polyester is around 36°C. Figure S2 shows that the viscosity of the polymer solution increases abruptly with the increase in temperature, reflecting the transformation of the polymer solution from sol to gel.

According to previous studies on the mechanism of gel formation, it is known that PEG polyesters can self-assemble in aqueous solutions to form micelles; with increasing temperature, hydrophobic interactions cause the micelles to aggregate and form a permeable gel network (*46*, *47*). This gel formation process of PEG polyesters does not require additional chemical cross-linking agents or ultraviolet (UV) light triggering, which can maximize the protection of the biological activity of siRNA. Moreover, our previous studies have shown that PEG polyesters are nonswelling and can be retained in vivo for more than 30 days, meaning they provide a good material basis for constructing antiadhesive patches that can be stably maintained in vivo (*48*). To clarify the effect of PEG polyester′s concentration on its phase transition temperature, we configured polymer solutions with a concentration gradient of 15 to 25 wt % and used the inverted tube method to obtain the phase diagram of the PEG polyester solution. As shown in Fig. 3J, the aqueous polymer solution underwent sol-gel phase transition with increasing temperature, and the phase transition temperature decreased with increasing polymer concentration. In addition, the biocompatibility of PEG polyester was determined by a Cell Counting Kit-8 (CCK-8) kit, as shown in Fig. 3K. Even when the concentration of PEG polyester was increased to 500 μg/ml, the proliferation viability of the cells did not show any statistical difference compared to the control group, which indicates the excellent biosafety of PEG polyesters.

Construction of lubricated gene-hydrogel patch

The lubricated gene-hydrogel patch was prepared as shown in Fig. 4A. PLGA electrospun membrane was prepared by the electrospinning technique, and then, PEI-PBA@ERK2-siRNA nanoparticles were loaded into an aqueous solution of PEG polyester and coated on the surface of the PLGA membrane. As shown in fig. S3A, the PLGA electrospun membrane can provide good mechanical support for the PEG polyester hydrogel, which allows the patch to be freely curled into a cylindrical structure with a composite tendon shape. From the stress-strain curves and tensile strength tests, we found that the mechanical properties of the lubricated gel patch were enhanced compared to the PLGA patch (fig. S3, B and C). In addition, the unique temperature-sensitive property of PEG polyester enables it to self-assemble into a hydrogel at body temperature, which can ensure the maximum biological activity of the loaded siRNA compared to the methods of triggering by UV light or adding additional chemical cross-linking agents. The patch morphology was further observed using a scanning electron microscope (SEM), as shown in Fig. 4B. The electrospun membrane side of the lubricated gene-hydrogel patch still exhibited an interlaced fibrous mesh structure. The gel layer showed that the PEG polyester hydrogel could be uniformly distributed on the surface of PLGA, and the gene nanoparticles were widely distributed in the gel layer of the patch.

As the water contact angle results of Fig. 4C and fig. S4 show, the PLGA electrospun fiber membrane was hydrophobic (129.52° ± 1.31°), the addition of the PEG polyester gel layer made the PLGA electrospun fiber film transition from hydrophobic to hydrophilic (21.12° ± 1.05°, $P < 0.05$), and the addition of gene nanoparticles did not change the hydrophilic properties of the PEG polyester layer. As shown in Fig. 4D, the lubricity of the patch was measured by a microdynamic wear tester. The coefficient of friction of the lubricated gene-hydrogel patch group was stable at 0.3897 ± 0.1719 during the 1500-s test, and the coefficient of friction of the nonlubricated layer control group was 1.3212 ± 0.1063, which proved that the proposed patch could form stable motion lubrication protection on the outer surface and effectively reduce the coefficient of friction by 70% (Fig. 4E).

Unidirectional release and anti-cell adhesion properties of lubricated gene-hydrogel patch

Given the double-layer structure of the patch and the hydrophobic property of PLGA, we believe that the proposed patch has unidirectional drug release capability. As shown in Fig. 5A, the unidirectional release of the lubricated gene-hydrogel patch was tested in Transwell plates, and the release experiments demonstrated that the presence of hydrophobic PLGA electrospun membrane could effectively prevent the release of the gene transfection complex to the fiber side. The enhanced fluorescence around the nuclei of the cocultured 208F cells on the gel side was observed on the third and fifth days under fluorescence microscopy, indicating that the 5-Carboxyfluorescein-labeled ERK2-siRNA was released from the gel side and taken up by the cells. However, the cells on the fiber side did not show any change in fluorescence intensity. The release curve in Fig. 5B further demonstrated the unidirectional release ability of the lubricated gene-hydrogel patch. The patch could release approximately 70% of the gene nanoparticles from the gel side within 12 days, suggesting that the lubricated gene-hydrogel patch can effectively mediate ERK2 gene silencing to inhibit fibroblast proliferation in the early stages of inflammation without influencing the healing area.

As shown in Fig. 5D, the porous structure of traditional electrospun patches allows for cell adhesion. In contrast, the lubricated gene-hydrogel patch exhibits excellent anti-cell adhesion performance, which is mainly because the ether bond on the surface of the hydrogel can form a stable lubrication layer and effectively prevent the adsorption of cell adhesion molecules. At the same

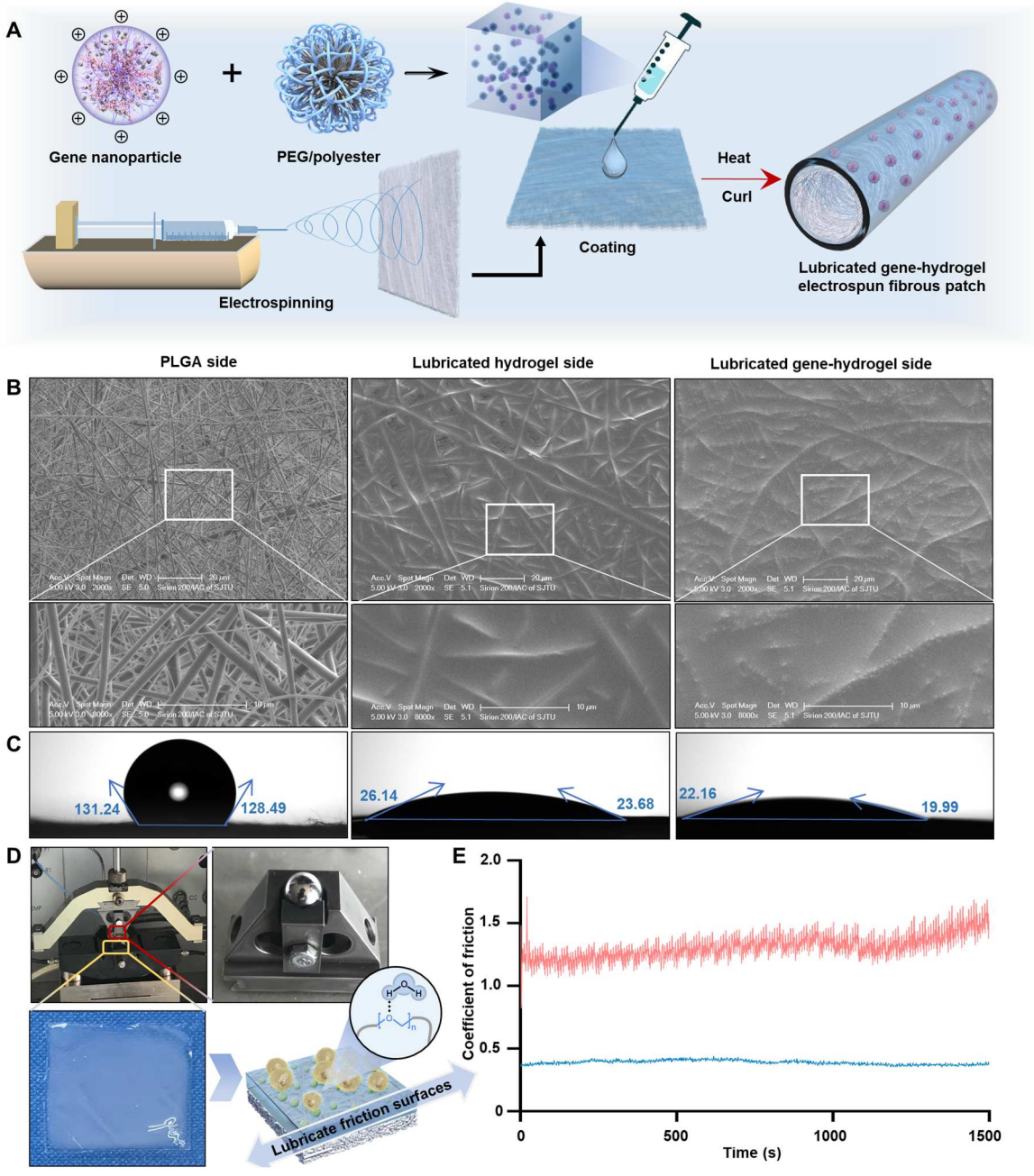

Fig. 4. Construction of lubricated gene-hydrogel patch and its characterization. (**A**) Fabrication of tendon sheath–like patch. (**B**) SEM micrographs of the lubricated gene-hydrogel patch from a different side. (**C**) Water contact angle of the lubricated gene-hydrogel patch from a different side. (**D**) Photograph and schematic of the lubricated gene-hydrogel patch. (**E**) Coefficient of friction-time curve for the lubricated patch (blue) and nonlubricated control group (red).

time, the gene nanoparticles carried in the PEG polyester hydrogel can play a synergistic role in reducing the production of adhesion tissue by inhibiting the signaling pathway of cell proliferation. As shown in Fig. 5 (C to E), we seeded 208F cells on different patches and stained the cytoskeletons and nuclei with ghost cyclopeptide (red) and 4′,6-diamidino-2-phenylindole (DAPI) (blue), respectively. Observing their growth status after 2 days of coculture, we found that, compared with the control and PLGA groups, the cell spreading area of the lubricated hydrogel patch group was reduced ($P < 0.0001$) and the cells of the lubricated gene-hydrogel patch group were changed from shuttle shape to round with the synergistic effect of gene nanoparticles, which proved that the presence of the PEG polyester lubrication layer could inhibit cell adhesion and mechanical activation, and gene silencing further enhanced this effect.

Optimization of gene silencing efficiency for preventing tendon adhesions

The biological factors leading to tendon adhesions are mainly attributed to the unique healing mechanism of tendons, which can

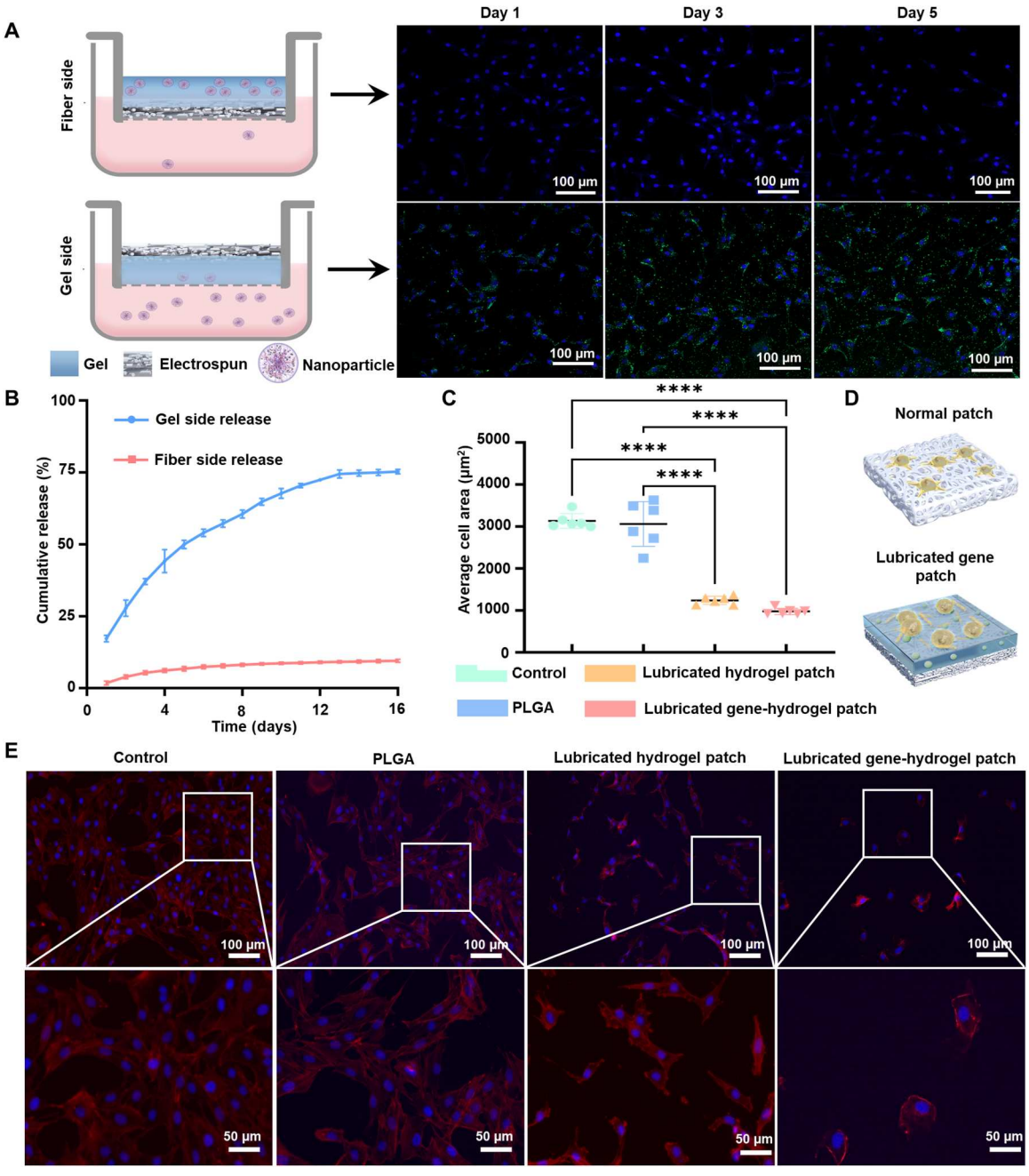

Fig. 5. Unidirectional release and anti-cell adhesion properties of lubricated gene-hydrogel patch. (**A**) Using Transwell plates to analyze the release and cell uptake of gene nanocomplex from a different side. (**B**) Cumulative release curve of gel and fiber side of lubricated gene-hydrogel patch for 12 days. (**C**) Average cell area of 208F cells seeded on different surfaces (mean ± SD, ****$P < 0.0001$, $n = 6$). (**D**) Schematic representation of cell morphology on different surfaces. (**E**) Fluorescence image of 208F cells seeded on different surfaces for 2 days. Red: cytoskeletons stained by phalloidin; blue: nuclei stained by 4′,6-diamidino-2-phenylindole (DAPI).

be divided into endogenous healing mediated by migration of the defective tendon cells and exogenous healing mediated by proliferation and invasion of external fibroblasts. The activation of the TGF-β1–ERK2–SMAD3 axis leads to fibroblast proliferation and increased secretion of collagen type III (COL III), which ultimately leads to tendon scar healing and adhesions. For this reason, targeting the silencing of ERK2 expression in fibroblasts is a powerful way to block the factors that trigger tendon adhesions.

To further optimize the transfection efficiency of PEI-PBA gene nanocomplex, we prepared four gene nanocomplex groups based on agarose gel electrophoresis data to investigate the effect of mass ratio on gene transfection (M = 1, 2, 3, and 4). The fluorescence intensity of intracellular siRNA increased with the increase of M (Fig. 6A). We further quantified the gene transfection efficiency by flow cytometry, as shown in Fig. 6B and fig. S5. The transfection efficiency of PEI-PBA@ERK2-siRNA gradually increased from

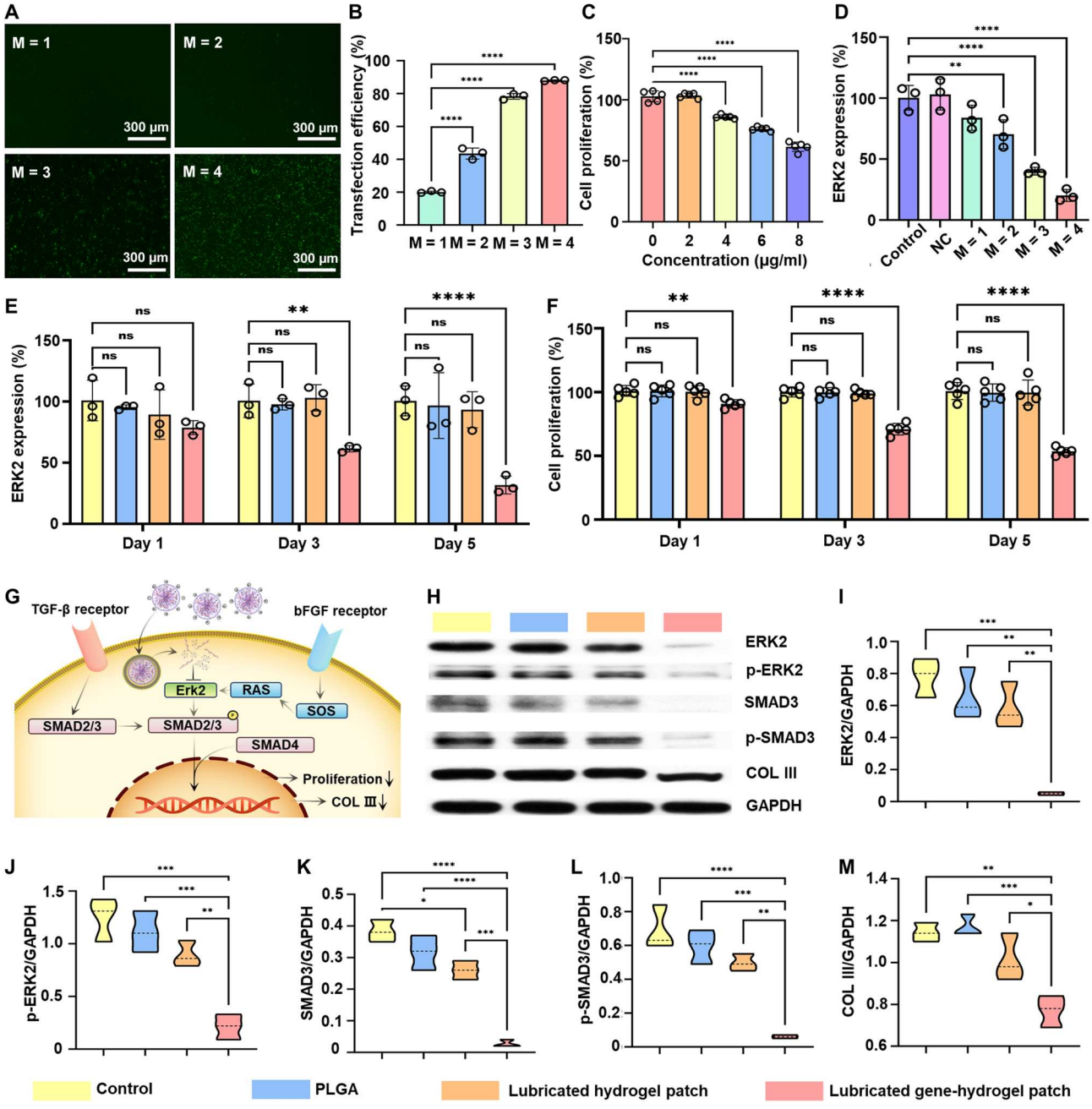

Fig. 6. The validation of molecular mechanism for prevention of tendon adhesions. (**A**) Fluorescence image of PEI-PBA@ERK2-siRNA with different *M* ratio–transfected 208F cells. Green: FAM-labeled siRNA. (**B**) Transfection efficiency of PEI-PBA@ERK2-siRNA with different *M* ratios (mean ± SD, ****$P < 0.0001$; $n = 3$). (**C**) Inhibition of cell proliferation efficiency of PEI-PBA@ERK2-siRNA with different *M* ratios (mean ± SD, ****$P < 0.0001$; $n = 5$). (**D**) Gene silencing efficiency of PEI-PBA@ERK2-siRNA with different *M* ratios (mean ± SD, **$P < 0.01$ and ****$P < 0.0001$; $n = 3$). NC, Negative Control. (**E**) Long-lasting gene silencing efficiency assessment of different patches for 5 days (mean ± SD, **$P < 0.01$ and ****$P < 0.0001$; $n = 3$). ns, not significant. (**F**) Long-lasting inhibition of cell proliferation efficiency of Control, Negative Control, and different *M* ratio patches for 5 days (mean ± SD, **$P < 0.01$ and ****$P < 0.0001$; $n = 3$). (**G**) Schematic diagram of ERK2-mediated tissue adhesion signaling pathway. (**H** to **M**) Western blotting analysis of expressions of ERK2, p-ERK2, SMAD-3, p-SMAD3, and COL III in 208F cells with different patches (mean ± SD, *$P < 0.05$, **$P < 0.01$, ***$P < 0.001$, and ****$P < 0.0001$; $n = 3$). GAPDH, glyceraldehyde-3-phosphate dehydrogenase.

20.07 ± 0.46% to 88.00 ± 0.28% ($P < 0.001$) as M gradually increased. The intracellular gene silencing efficiency of PEI-PBA@ERK2-siRNA was determined by quantitative reverse transcription polymerase chain reaction (qRT-PCR). As shown in Fig. 6D, the gene silencing efficiency was up to 79.81 ± 3.98% ($P < 0.001$) when $M = 4$, which indicated that PEI-PBA@ERK2-siRNA could effectively deliver ERK2-siRNA targeting to silence ERK2 gene expression intracellularly. Previous studies have shown that the strong cytotoxicity of PEI cationic carriers limits their application in the biomedical field. To verify the biocompatibility of PEI-PBA, we prepared complete media containing different concentrations of PEI-PBA and cocultured the media with 208F cells. The cell viability assay results are shown in Fig. 6C. When the concentration of PEI-PBA is less than 2 μg/ml, there is no substantial difference in cell viability compared with the control group, which indicates that the introduction of PBA moiety can notably reduce the cytotoxicity problem caused by the high orthoelectricity of PEI.

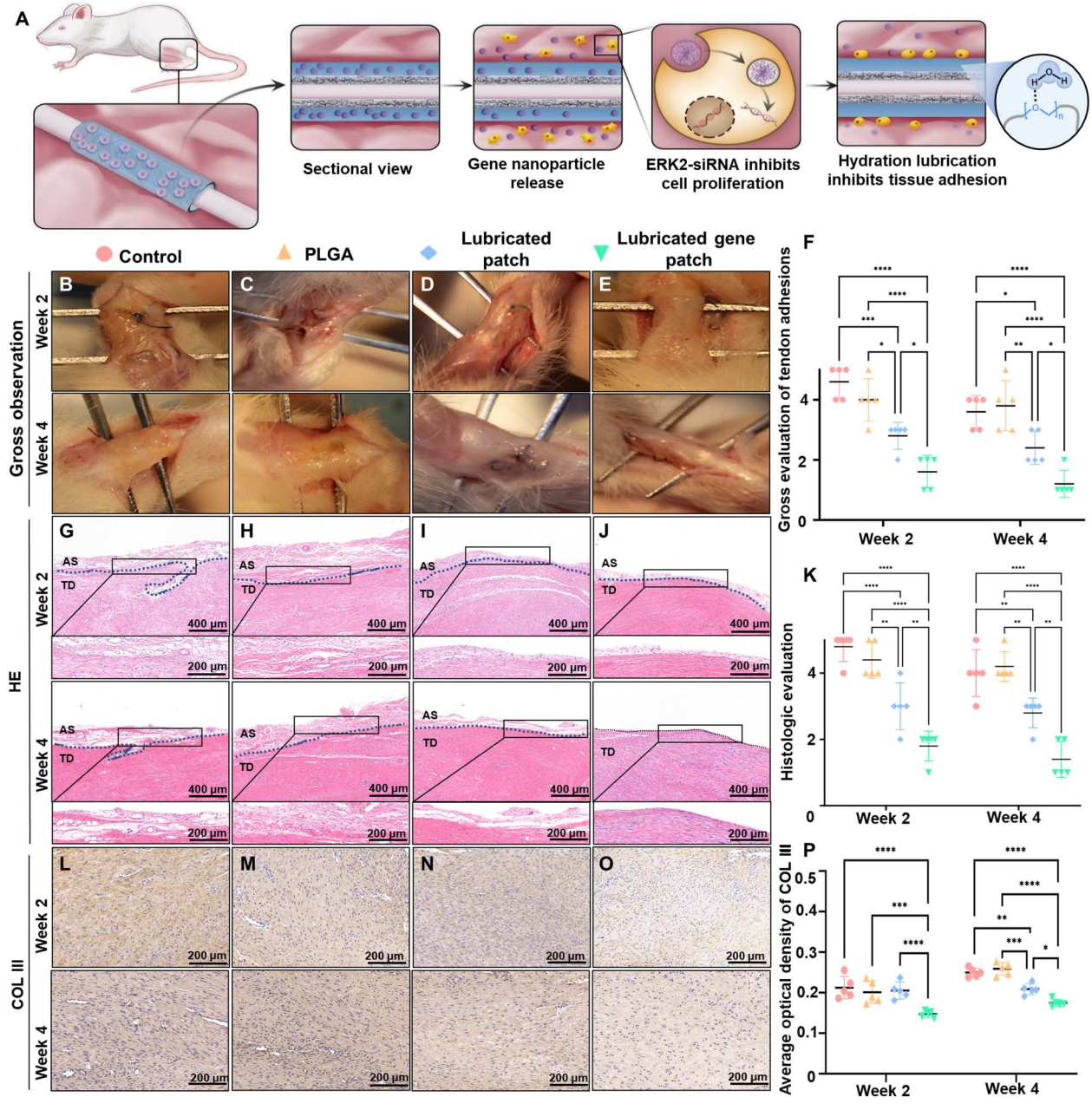

Fig. 7. Evaluation of lubricated gene-hydrogel patch in vivo. (**A**) Application of lubricated gene-hydrogel patch for peritendinous antiadhesion. (**B** to **E**) Gross observation of peritendinous adhesion of injured tendon at 2 and 4 weeks. (**F**) Gross scores of peritendinous adhesion (mean ± SD, $^{*}P < 0.05$, $^{**}P < 0.01$, $^{***}P < 0.001$, and $^{****}P < 0.0001$; $n = 5$). (**G** to **J**) H&E staining images of different patches. AS, adhesion areas; TD, repaired tendon site. (**K**) Histologic scores of peritendinous adhesion (mean ± SD, $^{**}P < 0.01$ and $^{***}P < 0.001$, and $^{****}P < 0.0001$; $n = 5$). (**L** to **P**) Immunohistochemical staining and evaluation of Col III expression in peritendinous tissue at 2 and 4 weeks (mean ± SD, $^{*}P < 0.05$, $^{**}P < 0.01$, $^{***}P < 0.001$, and $^{****}P < 0.0001$; $n = 5$).

To further verify the sustained gene silencing and cell proliferation inhibition efficiency of the lubricated gene-hydrogel patch, we cocultured 208F cells with lubricated gene-hydrogel patches for 1, 3, and 5 days before performing qRT-PCR and CCK-8 assay (Fig. 6, E and F). The results showed that PEI-PBA@ERK2-siRNA was released from the PEG polyester hydrogel during coculture and continued silencing the gene expression of cultured cells. We observed that the gene expression level of ERK2 did not change on the first day, and no decrease in cell proliferation was observed, which may have been caused by the fact that the siRNA had not yet exerted its physiological activity after being taken up by the cells. The expression level of ERK2 in the cells in the lubricated gene-hydrogel patch group decreased from the third day, followed by a slowdown in the cell proliferation rate, indicating that the PEI-PBA@ERK2-siRNA carried in the patch could effectively mediate intracellular gene silencing and inhibit fibroblast proliferation. In addition, the efficiency of gene silencing and proliferation inhibition was enhanced by the increasing number of gene nanoparticles released. The gene silencing efficiency of the lubricated gene-hydrogel patch could reach 68.26 ± 5.90% ($P < 0.001$), and the cell proliferation inhibition efficiency could reach 53.05 ± 2.67% ($P < 0.001$) after 5 days of coculture.

We further explored the protein expression of the TGF-β1–ERK2–SMAD3 axis by Western blotting (Fig. 6, G and H), and the results showed that 208F cells cocultured with the lubricated gene-hydrogel patch for 5 days had reduced expression of ERK2 and Phospho-ERK (p-ERK2) compared to the other three groups (Fig. 6, I and J). The patch with the motion lubrication layer effectively reduced the expression of SMAD3, which proved that the PEG polyester hydrogel can block the upstream signal of fibroblast mechanical activation. In addition, the reduced phosphorylation level of ERK2 directly blocked the phosphorylation transduction process of SMAD3 (Fig. 6, K and L), which, in turn, reduced the expression level of COL III (Fig. 6M). These results suggest that the lubricated gene-hydrogel patch can effectively silence intracellular ERK2 gene expression, thereby regulating the signaling of the TGF-β1–ERK2–SMAD3 axis and inhibiting fibroblast activation and proliferation and COL III deposition. To further verify the biocompatibility of the prepared patches, we cocultured the patch leachate with 208F cells and performed LIVE-DEAD staining. As shown in fig. S6, no cell death was observed in any group after 5 days of coculture, which demonstrated the excellent biocompatibility of the lubricated gene-hydrogel patch.

In vivo evaluation of the effect of lubricated gene-hydrogel patch

As shown in Fig. 7A, we sutured the ruptured tendon and subsequently wrapped it with a lubricated gene-hydrogel patch to prevent tendon adhesions. Adhesions were assessed by observing the surgical site of the Achilles tendon. The rat Achilles tendon model was divided into four groups: untreated control group, PLGA group, lubricated hydrogel patch group, and lubricated gene-hydrogel patch group. No infectious ulceration or necrosis occurred around the incision in any of the groups. At 2 weeks, the control group developed a large amount of adherent tissue in the surrounding area of the repair site, requiring sharp separation to expose the tendon, and the tendon injury area healed poorly with jelly-like deposits of adherent tissue. At 4 weeks, the adhesions of the peritendinous tissues were slightly improved, and the jelly-like collagen was more densely deposited on the tendon surface with a relatively smooth surface (Fig. 7B). The PLGA group still had unhealed severed ends in the injury area at 2 weeks, with an uneven surface that required sharp separation of the tendon from the peritendinous adherent tissue. At 4 weeks, the inflammation was reduced, and the tendon was completely healed, with a smoother surface than at 2 weeks but still with dense jelly-like adhesions (Fig. 7C). The lubricated hydrogel patch and lubricated gene-hydrogel patch groups had less adherent tissue on the tendon surface than the control and PLGA patch groups at 2 and 4 weeks due to the anticellular adhesion and lubrication effect of PEG polyester hydrogel (Fig. 7, D and E). Notably, compared with the lubricated hydrogel patch group, the lubricated gene-hydrogel patch group showed fewer surrounding adhesions, fewer tendon fibrosis, and better healing, suggesting that the in situ gene silencing effect of PEI-PBA@ERK2-siRNA inhibited the proliferation of fibroblasts and reduced the production of adhesions and the degree of peritendinous fibrosis. Subsequent gross evaluation of tendon adhesions revealed that the adhesions in the control and PLGA groups were mainly distributed between grades 4 and 5, with no statistical difference. The adhesions in the lubricated hydrogel patch group were mostly at grade 3, and this improvement was due to the hydrated antiadhesive layer. The lubricated gene-hydrogel patch group had the mildest adhesions due to the combined effect of in situ gene silencing and the hydrated antiadhesive layer, and its adhesion scores were lower than the other three groups, mainly distributed among grades 1 and 2 (Fig. 7F). Now, clinical drugs such as NSAIDs, rapamycin, and quercetin are widely used to reduce peritendinous adhesions by reducing inflammation, inducing apoptosis, and inhibiting oxidative stress. However, these drugs are not effective in blocking fibroblast overproliferation, which is a critical shortcoming because fibroblast overproliferation directly leads to tissue fibrosis. In this study, we developed an antiadhesion patch by applying targeted gene silencing technology to silence ERK2 to block the fibroblast proliferation process from the genetic level. Moreover, the hydrated lubricating layer composed of PEG polyester hydrogel has a notable effect on protecting the healing process of the injured area by shielding the adhesion sites and reconstructing the lubrication microenvironment. Therefore, the combination of ERK2 gene silencing with a lubricating antiadhesive layer reduced the extent of peritendinous adhesions.

Histological analysis was performed to further characterize the cause and extent of tendon adhesions. To analyze the effect of histopathological changes in the injured Achilles tendon, histological sections of the repaired area were stained with hematoxylin and eosin (H&E). As shown in Fig. 7, G to J, sections from the control group showed large numbers of adhesions on the tendon surface and invasion into the repaired area. However, the hydrated lubrication layer formed by the PEG polyester hydrogel reduced the adhesion on the tendon surface, and the treatment effect was further enhanced by the combination of ERK2-siRNA treatment, resulting in a smoother tendon surface. As shown in Fig. 7K, histological evaluation of the four groups showed that the lubricated gene-hydrogel patch group had a lower adhesion score than the other three groups.

Figure 7 (L to O) shows that COL III deposition was severe in the control, PLGA, and lubricated patch groups, which was due to the lack of effective targeting of bioactive substances to block COL III secretion in these three groups. In contrast, PEI-PBA@ERK2-

siRNA carried in the lubricated gene-hydrogel patch could be released continuously in the early inflammatory stage, regulating the signaling of the TGF-β1–ERK2–SMAD3 axis by knocking down ERK2 gene expression and reducing COL III deposition at the defect site ($P < 0.05$) (Fig. 7P). These results suggest that although the PEG polyester layer can reduce the adhesion of peritendinous tissues to some extent, it lacks a mechanistic treatment for blocking disease progression. However, by combining it with gene silencing therapy, it can block the disease progression mechanism and play a synergistic role in preventing tendon adhesions.

In vivo assessment of tendon healing status

We used double-label immunofluorescence staining to assess fibroblast proliferation, where α–smooth muscle actin (α-SMA) excites green fluorescence and vimentin excites red fluorescence. Vimentin is an important type III intermediate filament protein that is expressed only in fibroblasts, and increased red fluorescence indicates severe tissue fibroproliferation. Myofibroblast activation is characterized by the admixture of large amounts of α-SMA into stress fibers, and enhanced green fluorescence represents increased capillary angiogenesis (*49*).

As shown in Fig. 8 (A to D), a large number of vimentin-positive cells and α-SMA–positive cells were observed in the control, PLGA, and lubricated hydrogel patch groups 2 weeks after surgery, representing the appearance of neovascular tissue and the initiation of the fibrosis process in the tendon injury. The control and PLGA patch groups showed much more vimentin-positive cells than the lubricated hydrogel patch group, whereas no notable vimentin-positive or α-SMA–positive cells were observed in the lubricated gene-hydrogel patch group. As shown in the optical density semiquantitative results of Fig. 8 (I and J), the fibrosis and vascularization levels in the lubricated gene-hydrogel patch group were significantly lower than those in the other three groups ($P < 0.001$).

As shown in Fig. 8 (E and H), the vimentin-positive cells and α-SMA–positive cells in the control, PLGA, and lubricated hydrogel patch groups remained at higher levels at 4 weeks postoperatively, suggesting a shift in tendon healing toward fibrotic scar healing. Small numbers of vimentin-positive cells and α-SMA–positive cells were also observed in the lubricated gene-hydrogel patch group, which may have been due to the fact that PEI-PBA@ERK2-siRNA in PEG polyesters had been completely released, and the gene silencing effect on adherent cells was reduced. As shown in Fig. 8 (J and L), the optical density semiquantitative results showed that the fibrosis and vascularization levels in the lubricated gene-hydrogel patch group were still lower than that in the other three groups. At the same time, we found that the fibrosis and vascularization levels in the lubricated hydrogel patch group were lower than those in the control and PLGA patch groups, which proved that the motion lubrication layer can effectively block the mechanical activation of fibroblasts and reduce the fibrosis and vascularization levels.

Immunofluorescence staining demonstrated that inhibiting fibroblast activation and proliferation at the early stage of inflammation and constructing an anti-cell adhesion hydrogel layer could effectively block the ERK2-mediated TGF-β1–ERK2–SMAD3 axis-induced fibrosis and vascularization in tendons by acting synergistically from both biological and physical aspects.

The assessment of tendon motion and biomechanical function

After 4 weeks postoperatively, we assessed the Achilles tendon motion function in the control group, PLGA group, lubricated patch group, and lubricated gene patch group by gait analysis. As shown in Fig. 9, the Achilles functional index (AFI) in all four experimental groups decreased with different degrees, and the AFI scores of lubricated patch and lubricated gene patch were higher than the control group, suggesting that the patch with lubricating properties could effectively improve the motor function of the Achilles tendon, and in addition, ERK2-siRNA effectively inhibited the deposition of peritendinous adhesion tissue and tendon fibrosis.

As shown in Fig. 10A, to further evaluate the tendon healing strength and whether ERK2-siRNA in the lubricated gene patch interferes with the normal tendon healing process, we systematically tested the elastic modulus, stiffness, maximum tensile stress, and maximum tensile load of the tendon at 2 weeks postoperatively. In the results shown in Fig. 10 (B to E), the biomechanical properties of control group, PLGA group, lubricated patch group, and lubricated gene patch did not show notable differences, and the biomechanical properties of lubricated gene patch group showed a slight improvement compared with other groups but not statistically different. This demonstrates that reducing tendon adhesions by inhibiting the exogenous healing process does not lead to a decrease in tendon strength of the tendon itself. Maximizing protection of the endogenous healing process of the tendon is a potential way to achieve adhesion-free healing of the tendon.

The assessment of gene and protein expression

To further determine the effect of different types of patches on collagen production at the tendon healing site, we performed qPCR and Western blot assays on the tendon injury site at 2 weeks postoperatively. qPCR results are shown in fig. S7. The collagen deposition in the lubricated patch and lubricated gene patch groups was less than that in the control, and this may be due to the presence of lubricated layer, which effectively blocked the invasion of exogenous fibroblasts to the injury site. In addition, there was a slight decrease in ERK2 expression in the lubricated gene patch group compared with the control and PLGA groups, which may be due to the infiltration of a very small amount of ERK2-siRNA into the tendon injury.

The results of Western blot were shown in fig. S8, which were consistent with the results of qPCR. The lubricated patch group and lubricated gene patch group showed different degrees of decreased collagen expression, while the expression level of ERK2 did not differ between groups, which proved that our designed lubricated gene patch could effectively reduce the release of ERK2-siRNA to the inner layer of the fiber membrane and ensure the endogenous healing process of tendon to the maximum extent. As shown in fig. S9, we further evaluated the ratio of COL I to COL III at the tendon injury, and we found that the ratio of COL I/COL III in the lubricated gene patch group was higher compared to the control group, indicating that the tendon healing was no longer a scar-type healing with predominantly adherent tissue.

DISCUSSION

Several drugs and delivery systems have been developed to address the problems of adhesion and fibrosis in the tissue healing process

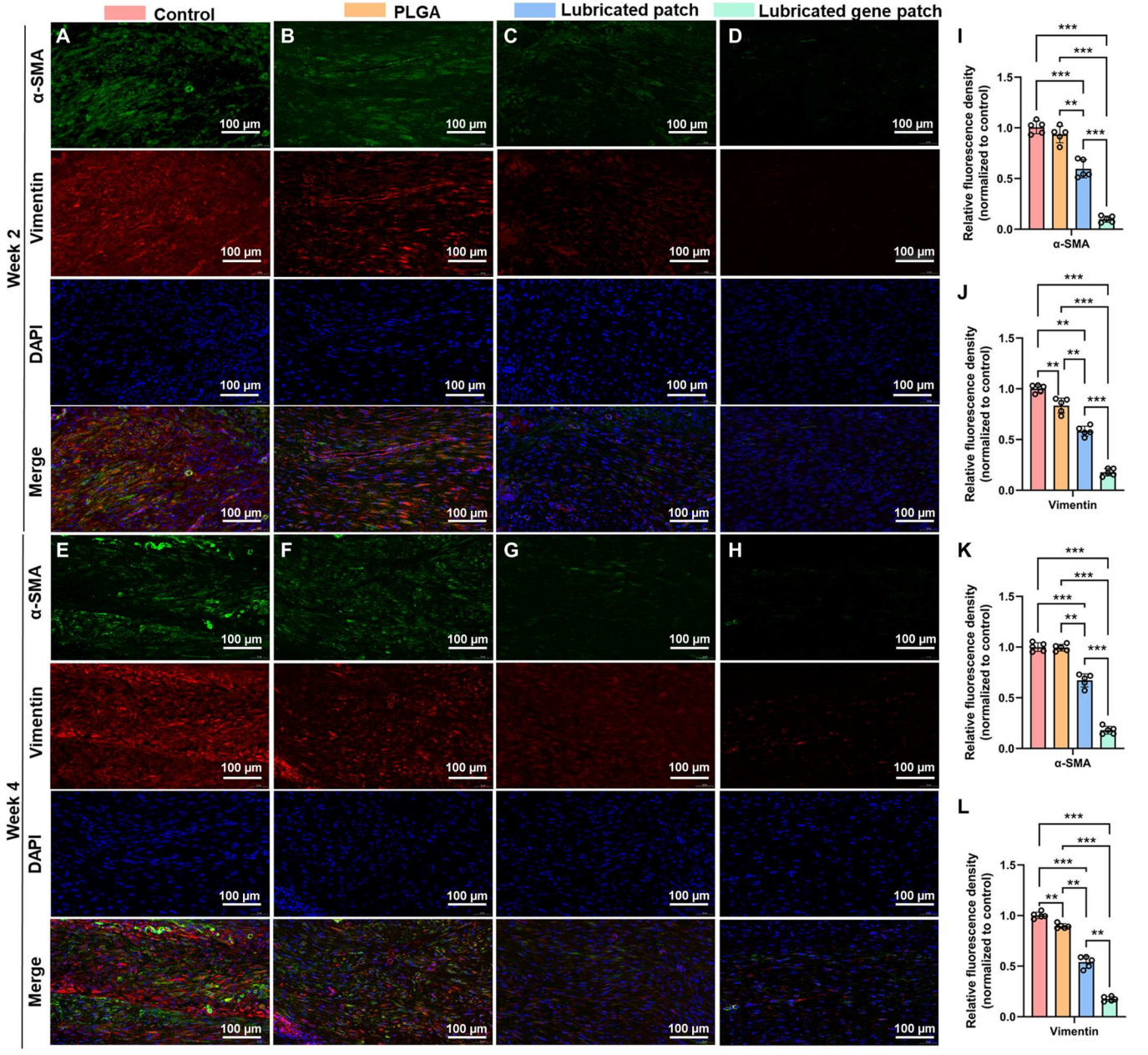

Fig. 8. Fibrosis and vascularization assessment of healing tendons. (**A** to **D**) Immunofluorescence double staining of α-SMA (green) and vimentin (red) at 2 weeks. (**E** to **H**) Immunofluorescence double staining of α-SMA (green) and vimentin (red) at 4 weeks. (**I** and **J**) Semiquantitative analysis on optical density of α-SMA and vimentin (mean ± SD, ***$P < 0.001$ and ****$P < 0.0001$; $n = 5$). (**K** and **L**) Semiquantitative analysis on optical density of α-SMA and vimentin (mean ± SD, **$P < 0.01$ and ***$P < 0.001$, $n = 5$).

(*20*, *50*–*54*). These therapeutic approaches can block disease signaling by inhibiting molecular mechanisms, but they often do not address the problem of abnormal intracellular gene or protein expression because of the physical environment. The mechanical activation of fibroblasts involves the following steps. First, fibroblasts adhere to the extracellular matrix, allowing cell resolution sensing. Second, fibroblasts bind to TGF-β1 latent in the extracellular matrix. Last, high levels of TGF-β1 signaling and mechanical stimuli such as friction led to activation. The use of a global anti–TGF-β1 strategy has off-target effects and exacerbates the inflammatory response (*55*, *56*). Combining accurate gene therapy and local motor lubrication environment reconstruction to block TGF-β1 signaling and reduce mechanical stimulation may be a promising therapeutic approach to avoid mechanical activation of fibroblasts (*2*).

Surface modification of fiber membranes by hydrogels is a proven method to change the surface characteristics of membranes. In a previous study, we successfully fabricated anti-cell adhesion electrospun fiber membranes by using peptide-modified method (*57*). In addition, we found that the porosity of the fiber membrane

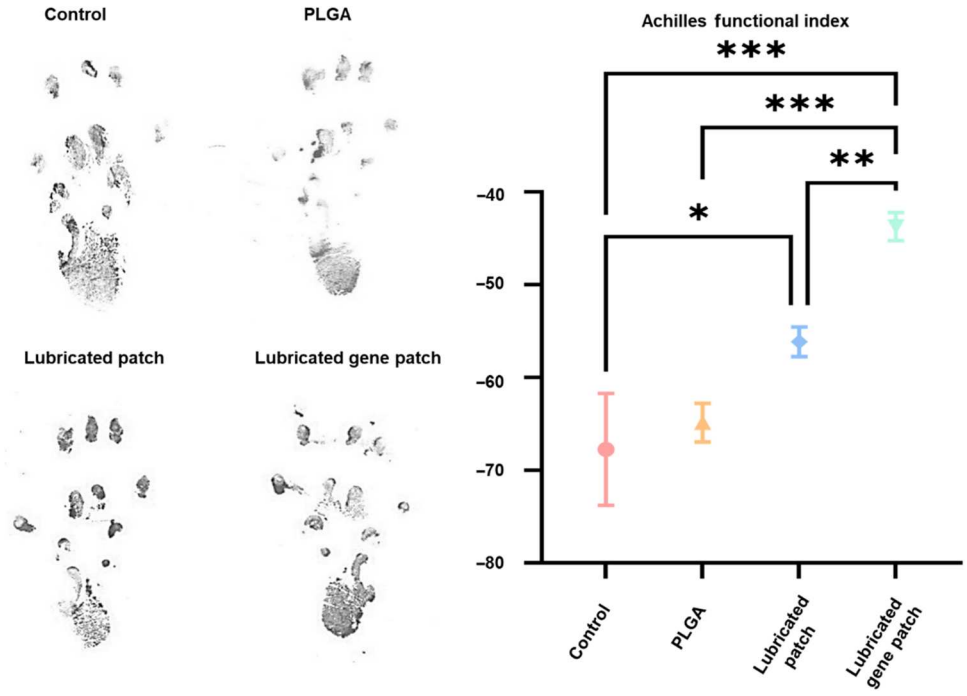

Fig. 9. Assessment of Achilles tendon motor function. Assessment of AFI in control, PLGA, lubricated patch, and lubricated gene patch groups after 4 weeks of Achilles tendon injury (*P < 0.05, **P < 0.01 and ***P < 0.001).

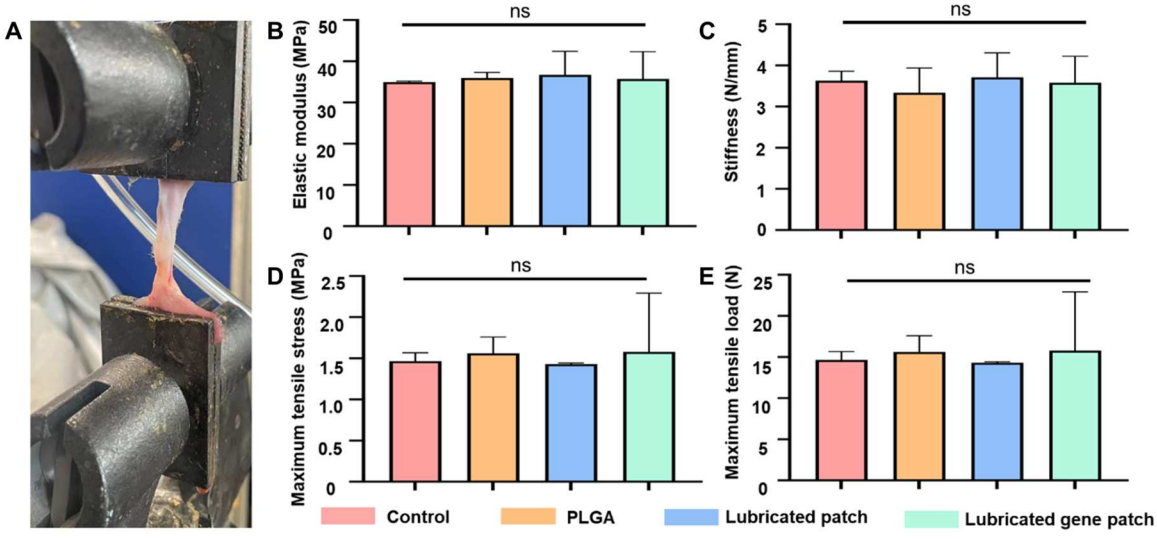

Fig. 10. Biomechanical testing of the rat Achilles tendon. (**A**) Photograph of Achilles tendon mechanics test. (**B**) Comparison of elasticity modulus between experimental groups. (**C**) Comparison of stiffness between experimental groups. (**D**) Comparison of maximum tensile stress between experimental groups. (**E**) Comparison of maximum tensile load between experimental groups.

surface affects cell adhesion and proliferation behavior (*58*). Therefore, we wanted to further investigate the surface properties of the material on the alteration of cell behavior and conducted a systematic study of fibroblast behavior in a lubricated environment. We were surprised to find that the activation of fibroblasts and the adhesion and fibrosis of tendons could be reduced by constructing lubricated materials, and we believe that this idea can be extended to most of the applications such as anti-adhesion and inhibition of implant material envelope formation.

In this study, we constructed a lubricated gene-hydrogel patch by integrating upstream and downstream signals that lead to mechanical activation of fibroblasts. The outer PEG polyester hydrated lubrication layer could effectively mimic the motion lubricating function of the tendon sheath and serve as a gene delivery library

for up to 12 days of gene silencing in vivo. In the 1500-s friction test, the motion lubrication layer reduced motion friction by 70% and did not show performance degradation throughout the test period, which proved that it can rebuild a stable motion lubrication environment. In addition, the unidirectional release of PEI-PBA@ERK2-siRNA nanoparticles can efficiently target intracellular ERK2-mRNA, knocking down 79.81 ± 3.98% of ERK2 gene expression, inhibiting 53.05 ± 2.67% of fibroblast proliferation, and reducing COL III deposition in tissues by more than 30%. Therefore, this lubricated gene-hydrogel patch combining reconstruction of motion lubrication environment to reduce mechanical stimulation of fibroblasts and gene therapy to silence the key gene expression of mechanical activation has great clinical value as an anti-adhesive patch. However, our study leaves something to be desired, such as our use of ERK2-siRNA to inhibit the production of peritendinous adhesion tissue, but lacks the ability to provide specific biosignal stimulation to the tendon defect site to further accelerate healing. How to find out the signaling pathways targeting tendon cell regeneration by single-cell sequencing and multiomics combination will be our future research and investigation.

MATERIALS AND METHODS

Materials

PEG [molecular weight (MW) = 1500], gelatin from porcine skin, and branched polyethylenimine with an MW of 25,000 were purchased from Sigma-Aldrich. 1,1,1,3,3,3-Hexaffuoro-2-propanol (HFIP) was purchased from Aladdin Industrial Co. Ltd. (Shanghai, China). LA and GA were purchased from Hangzhou Medzone Biotech Ltd. (Zhejiang, China). PLGA was purchased from Jinan Daigang Biomaterial Co. Ltd. (Jinan, China). 4-(Bromomethyl) phenylboronic acid (≥98%) was purchased from Macklin. ERK2-siRNA sequences were designed and synthesized by Genomeditech (Shanghai, China). Sequences of siRNAs (5′-3′) were 5′-GATCCG-CACCTCAGCAATGATCATATTCCTGTCAGAATGAT-CATTGCTGAGGTGCTTTTTG-3′. Dulbecco′s modified Eagle′s medium (DMEM), trypsin, fetal bovine serum (FBS), and antibiotics were purchased from Invitrogen (CA, USA).

Synthesis and characterization of PEG polyester

The detailed preparation method has been reported in a previous study (*48*). Briefly, 15 g of PEG (0.01 mol) was weighed into a dry flask and evacuated under an oil bath at 150°C for 3 hours to remove the water from the PEG. After the temperature of the three-necked flask was cooled to 120°C, under argon protection, a certain amount of LA and GA was added. Subsequently, the reaction system was evacuated and passed through argon gas at 80°C and repeated three times to eliminate the residual water in the monomers. After all monomers were melted, $Sn(Oct)_2$ (0.2 wt % monomer) was added, and the reaction system was mechanically stirred at 150°C under argon protection for 12 hours. After the reaction, the reaction products were washed three times by pouring into water at 80°C to remove unreacted monomers and low MW products. Residual water was removed by freeze drying, and the product was collected and stored at −20°C. Then, ^{1}H NMR (Bruker, 400 MHz, AVANCE III HD) was used to characterize the average MW (Mn) of the polymer and the composition ratio of the monomers. All ^{1}H NMR solvents were deuterated chloroform ($CDCl_3$), and tetramethyl silane was used as an internal standard at 25°C. GPC (Agilent 1260) characterization provided information on the MW and MW Distribution of the polymers. Narrowly distributed polystyrene was used as the standard sample, and tetrahydrofuran was used as the mobile phase. DMEM containing 10% FBS and PEG polyester (5, 25, 50, 250, and 500 μg/ml) was prepared and cocultured with 208F cells. After 1, 3, and 5 days, the CCK-8 kit (Beyotime Biotechnology, China) was used to determine the proliferation rate of 208F cells in each group to assess the biocompatibility of PEG polyester.

Characterization of PEG polyester hydrogels

The sol-gel phase transition of PEG polyester solutions was studied by the inverted tube method. A PBS solution of polymer (pH 7.4) with a concentration gradient of 15 to 25 wt % was prepared, and 0.5 ml was added to a sample bottle with an inner diameter of 8 mm after complete dissolution of PEG polyester in PBS by vortex shaking. The PEG polyester solution was in a flowable sol at room temperature, and the sample bottle was placed in a circulating water bath at an initial temperature of 30°C, kept at a constant temperature for 10 min, and then inverted in the water bath for 30 s to observe the state of the solution. If flowable, then the polymer solution at this temperature was a sol; if not flowable, then it was a gel. The above operation was repeated for every 1°C increase. A strain-controlled rheometer (Kinexus PRO, Malvern) equipped with a Peltier cone plate (cone: 1°, diameter: 60 mm, gap: 0.03 mm) was used to study the sol-gel phase transition behavior of a PBS solution of 25 wt % polymer PEG polyester. The variation of viscosity (η), energy storage modulus (G'), and loss modulus (G'') of the polymer/water system with temperature was investigated at an angular oscillation frequency of 10 rad/s, strain in the linear viscoelastic range (0.5%), and a ramping rate of 0.5°C/min.

Synthesis and characterization of PEI-PBA

One hundred milligrams of PEI was added to a dry round-bottom flask, and 2 ml of anhydrous dimethyl sulfoxide (DMSO) was added to dissolve it completely. Next, 250 mg of PBA was dissolved in 2 ml of anhydrous DMSO. The PBA was slowly added dropwise to the PEI solution under an oil bath at 60°C for 24 hours. After the reaction, the product was dialyzed in PBS for 3 days. The chemical structure and composition of PEI-PBA were confirmed by dissolving it in D_2O by 600-MHz ^{1}H NMR spectroscopy (Bruker, AVANCE III HD). DMEM medium with 10% FBS containing PEI-PBA (2, 4, 6, and 8 μg/ml) was prepared and cocultured with 208F cells, and CCK-8 assay was performed on days 1, 3, and 5 to show the proliferation rate of each group of 208F cells (American Type Culture Collection, USA) to test the biocompatibility of PEI-PBA.

Fabrication of PEI-PBA/siRNA complexes

PEI-PBA and ERK2-siRNA dissolved in diethyl pyrocarbonate–treated water were mixed at different mass ratios [$M = M_{(\text{PEI-PBA})}/M_{(\text{ERK2-siRNA})}$] and incubated for 30 min at room temperature to form gene transfection complexes. The binding ability of PEI-PBA to ERK2-siRNA was verified by agarose gel electrophoresis (Beyotime Biotechnology, China). Samples were run on a 3% (w/v) agarose gel at 70 V for 30 min. The resulting gel red–stained gels were photographed with bands by the UVI Pro Gel Documentation System (Tanon 2500, China). The particle size and zeta potential of PEI-PBA@ERK2-siRNA complexes were determined by

dynamic light scattering at 25°C using a Malvern Zetasizer Nano ZS90 (Malvern, UK).

Transfection efficiency, gene silencing efficiency, and proliferation inhibition of PEI-PBA@ERK2-siRNA

208F cells were inoculated in 24-well plates (Corning, USA) at a density of 4×10^5 to 5×10^5 per well. PEI-PBA was incubated with siRNA dissolved in diethyl pyrocarbonate water at room temperature for 30 min at different mass ratios, and the transfection solution was prepared with DMEM containing 10% FBS at a final concentration (siRNA) of 50 nM. After the cells completely adhered to the wall, 500 μl of the prepared transfection solution was added to each well and coincubated for 6 hours. The nuclei were stained with DAPI (Beyotime Biotechnology, China). For flow cytometry, cells were digested from the plates with trypsin and collected into polystyrene flow cytometry tubes to quantify FAM-siRNA cell uptake. Western blotting was performed to study the expression of ERK2 (p-ERK2), SMAD3 (p-Smad3), and COL III, with glyceraldehyde-3-phosphate dehydrogenase (GAPDH) as an internal control. Briefly, groups of repaired peritendinous tissues were separated in 100 μl of radioimmunoprecipitation assay (Beyotime Biotechnology, China) and homogenized for 30 min. Total protein concentration was measured using the dicinchoninic acid assay (Solarbio, China), and equal amounts of protein samples (10 μg per lane) were separated and transferred to polyvinylidene difluoride membranes. The following primary antibodies were used: GAPDH (ab181602), β-actin (ab8227), anti-ERK2 (ab32081), anti–p-ERK (ab201015) (1:1000; Abcam, UK), anti-SAMD3 (9523), anti–p-SMAD3 (9520), anti–COL III (98908), and anti–COL I (72026) (1:1000; Cell Signaling Technology, USA). After primary antibody incubation, membranes were incubated in goat anti-rabbit immunoglobulin G (Heavy and Light chain) horseradish peroxidase coupling (1:2000; Proteintech) for 2 hours at room temperature. Proteins were visualized, and images were captured using the LI-COR Odyssey Imager (LI-COR Biosciences, Lincoln, NE). Results were expressed as ERK2, p-ERK, SAMD3, p-SMAD3, COL III, and COL I levels and normalized to GAPDH or β-actin bands by optical densitometry in ImageJ. 208F cells containing FAM-labeled siRNA complexes were cocultured with PEI-PBA (giving rise to PEI-PBA@siRNA) in 24-well plates for 1, 3, and 5 days. The proliferation rate of each group of 208F cells was displayed by CCK-8 assay according to the manufacturer′s protocol. The results were expressed using the proliferation rate by normalizing the mean absorbance values at each corresponding time point to the control group. Each sample was tested five times.

Preparation of PLGA electrospun membrane

The spinning solution of PLGA was prepared by dissolving 1 g of PLGA in 10 ml of HFIP. The spinning solution was transferred into a 10-ml syringe (needle size, 22 gauge). The voltage was set to 18 kV, the distance of the nozzle from the collection device was 20 cm, and the flow rate of the spinning solution was 1 ml/hour. The obtained electrospun silk film was placed in a vacuum-drying oven overnight.

Preparation, contact angle, and drug release evaluation of lubricated gene-hydrogel patch

The PEI-PBA@FAM-siRNA was comixed with PEG polyesters and preheated at 30°C for 10 min to reduce its liquidity. Then, the mixture hydrogel was transferred to a horizontally placed PLGA membrane, while the membrane was placed in a 37°C thermostat for 2 min to prepare lubricated gene-hydrogel patches. The prepared patches were used to evaluate the release of siRNA. First, the patches were placed in the upper chamber of the Transwell cell culture plate, and the release level was assessed by adding an appropriate amount of 1× PBS to the lower chamber. A constant temperature of 37°C was maintained throughout, the PBS in the lower chamber was changed every 24 hours, and the fluorescence intensity in the solution was measured by a fluorescent enzyme marker. The concentration was calculated by measuring the fluorescence intensity of known concentrations of PEI-PBA@FAM-siRNA to draw a standard curve. The contact angles of the prepared patches were determined by a contact angle meter (Biolin Scientific). The patch surface morphology was observed using a SEM (Sirion 200).

In vitro evaluation of the lubricity, anti-cell adhesion, gene silencing efficiency, and cell proliferation inhibition of lubricated gene-hydrogel patch

The lubricity properties of the lubricated gene-hydrogel patches were characterized by a high-temperature microdynamic wear tester (Optimal Instruments, USA). The prepared patches were placed on a sample table at a controlled temperature of 37°C, a friction frequency of 1 Hz, an amplitude of 4 mm, a load of 1 N and run for 1500 s, and the experimental data were recorded. Then, the patches were spread on the bottom of 24-well plates and inoculated with 208F cells, which were cocultured with the patches for 48 hours. The cytoskeletons and nuclei were stained using actin staining and DAPI staining, respectively, and the cell-spreading area was assessed. Then, 208F cells were inoculated in the lower chamber of a 24-well Transwell cell culture plate (Corning, USA), and the upper chamber was loaded with lubricated gene-hydrogel patches to coculture the cells and patches. The nuclei were stained with DAPI on days 1, 3, and 5 to detect siRNA release. Gene silencing efficiency was detected using qRT-PCR. The proliferation rate of each group of 208F cells was measured by CCK-8 assay according to the manufacturer′s protocol. The results were expressed using the proliferation rate by normalizing the mean absorbance value for each corresponding time point to the control.

Rat Achilles tendon adhesion model

The animal experiment was approved by the Animal Research Committee of Shanghai Jiaotong University School of Medicine (SYXK 2018-0027). Animal models were established according to the previously reported procedures (*59*). Sprague-Dawley rats weighing 200 to 250 g were used as animal models for peritendinous adhesions. The hindlimbs of male rats were sterilized, and peritendinous adhesions were modeled by repairing the damaged Achilles tendon using a modified Kessler technique and 6-0 nonabsorbable sutures (Ethicon Ltd., Edinburgh, UK). The animals were randomly divided into four groups (n = 10 per group), and the animals were taken at 2 and 4 weeks. The control group did not receive any treatment, whereas the three experimental groups—the PLGA patch group, the lubricated hydrogel patch group, and the lubricated gene-hydrogel patch group—had the Achilles tendon suture wrapped with 1 cm by 2 cm of different formulations of the patch.

Gross evaluation

At 14 and 28 days after surgery, the rats were observed for signs of wound infection in the extremities. The hindlimb was incised longitudinally to expose the repaired Achilles tendon. On the basis of the surgical findings, grades 1 to 5 were quantified to assess the degree of peritendinous adhesions as follows (*20*): grade 1, no obvious adhesions on the tendon surface; grade 2, a small percentage of adhesions could be easily separated from the tendon by blunt dissection; grade 3, less than 50% of the adhesions could be separated with a blunt instrument; grade 4, 51 to 97.5% of the adhesions could be separated with a scalpel; and grade 5, more than 97.5% of the adhesions could be separated with a scalpel (all tendon status assessments were carried out during the sampling phase by three experimentalists for each animal model, and the final conclusions were reached after assessment and discussion).

Histologic evaluation

The tendon-bone ends and the muscle ends of the Achilles tendon were cut to separate the Achilles tendon tissue, which was fixed in paraformaldehyde for 1 day. Afterward, the samples were cut into 5-μm-thick sagittal sections. Sections were stained with H&E and immunohistochemical staining of type III collagen. The stained sections were observed under a light microscope (Leica DM6000). The adhesion histological scoring system was used to classify the repair site into grades 1 to 5 as follows (*20*): grade 1, no adhesions in the peritendinous area of the repair site; grade 2, less than 25% adhesions in the peritendinous area of the repair site; grade 3, 25 to 50% adhesions in the peritendinous area of the repair site; grade 4, 50 to 75% adhesions in the peritendinous area of the repair site; and grade 5, more than 75% adhesions in the area of the repair site.

Immunofluorescence

Paraffin sections were dewaxed to water, and antigenic repair was performed using citric acid, while bovine serum albumin was used for closure afterward. Next, α-SMA + vimentin primary antibody (Servicebio China) was added dropwise to the area to be tested and incubated overnight at 4°C. The area to be tested was incubated with Alexa Fluor 488 goat anti-mouse (α-SMA) + CY3-goat anti-rabbit (vimentin) secondary antibody for 50 min, followed by observation under a fluorescence microscope.

Gait analysis

Animals were tested in a restricted corridor with dark masking at the end. An 8 cm–by–42 cm sheet of photocopy paper (dipped in acetone solution containing 0.5% anhydrous bromophenol blue) was laid on the corridor floor. The rats were grasped by the thorax, their hind paws were dipped into a tray with a water-soaked sponge, and they were allowed to walk down the corridor, leaving blue footprints on the paper. The paper was coded with the animal number and stored in a dark room for subsequent measurements. The distance relative to the foot (TOF), the footprint length (PL), the distance between the first and fifth toes or toe extension (TS), and the distance between the second and fourth toes or intermediate toes (IT) were measured and recorded the longest measurement for each parameter on both sides (where the left side is undamaged and is the normal control, and the right side for the group to be measured). We recorded the measurements of all footprints on each strip of paper (printed range of four to eight footprints per sheet) and calculated the mean value for each parameter. The coefficient of variance of the AFI measured using the mean was less than the coefficient of variance of the longest measurement. A factor was generated for each of the following measurements

$$\text{Distance to opposite foot factor (TOFF)} = (\text{ETOF} - \text{NTOF})\text{NTOF}$$

$$\text{Print length factor (PLF) for de Medinaceli} = (\text{NPL} - \text{EPL})/\text{EPL}$$

$$\text{Total toe width factor (TSF)} = (\text{ETS} - \text{NTS})/\text{NTS}$$

$$\text{Distance between intermediate toes factor (ITF)} = (\text{EIT} - \text{NIT})/\text{NIT}$$

TS is the total toe width, PL is the print length, IT is the distance between the middle toes, TOF is the distance to the opposite foot, N is the normal uninjured side, and E is the experimental side.

$$\text{AFI} = 74\ \text{PLF} + 16\ \text{TSF} + 48\ \text{ITF} - 5$$

Biomechanical evaluation

Biomechanical evaluation was performed at 2 weeks after surgery. Rats were executed by intraperitoneal injection of 2% sodium pentobarbital (100 mg/kg), the left and right hindlimbs were incised from the distal and proximal ends, about 1 cm of peritendinous tissue above and below the surgical site of the Achilles tendon was excised, and the maximum tensile force for Achilles tendon rupture (Fig. 10A) was tested by biomechanical experiments using a tensile tester at proximal end. The biological strength of the repaired tendon was evaluated with a longitudinal load. The device was pulled at a constant speed of 1 mm/min, the tensile load (N) was gradually increased until the tendon ruptured from the suture, and the results were entered into TRAPEZIUM X 13.0 mechanical analysis software.

Statistics analysis

All data were recorded as mean ± SD. Comparisons between the two groups were measured by the Student's *t* test, comparisons for more than two groups were measured by one-way analysis of variance (ANOVA), and $P < 0.05$ was considered to indicate statistical significance.

Supplementary Materials

This PDF file includes:

Table S1
Figs. S1 to S9

View/request a protocol for this paper from *Bio-protocol*.

REFERENCES AND NOTES

1. C. N. Fortin, G. M. Saed, M. P. Diamond, Predisposing factors to post-operative adhesion development. *Hum. Reprod. Update* **21**, 536–551 (2015).

2. N. Noskovicova, R. Schuster, S. van Putten, M. Ezzo, A. Koehler, S. Boo, N. M. Coelho, D. Griggs, P. Ruminski, C. A. McCulloch, B. Hinz, Suppression of the fibrotic encapsulation of silicone implants by inhibiting the mechanical activation of pro-fibrotic TGF-β. *Nat. Biomed. Eng.* **5**, 1437–1456 (2021).
3. M. L. Killian, L. Cavinatto, L. M. Galatz, S. Thomopoulos, The role of mechanobiology in tendon healing. *J. Shoulder Elbow Surg.* **21**, 228–237 (2012).
4. C. Zhao, Y. Ozasa, R. L. Reisdorf, A. R. Thoreson, G. D. Jay, K. N. An, P. C. Amadio, CORR® ORS Richard A. Brand Award for Outstanding Orthopaedic Research: Engineering flexor tendon repair with lubricant, cells, and cytokines in a canine model. *Clin. Orthop. Relat. Res.* **472**, 2569–2578 (2014).
5. C. A. Beadles, A. D. Meagher, A. G. Charles, Trends in emergent hernia repair in the United States. *JAMA Surg.* **150**, 194–200 (2015).
6. J. F. Gillion, D. Sanders, M. Miserez, F. Muysoms, The economic burden of incisional ventral hernia repair: A multicentric cost analysis. *Hernia* **20**, 819–830 (2016).
7. K. M. Usher, S. Zhu, G. Mavropalias, J. A. Carrino, J. Zhao, J. Xu, Pathological mechanisms and therapeutic outlooks for arthrofibrosis. *Bone Res.* **7**, 9 (2019).
8. C. Cao, F. Wu, X. Niu, X. Hu, J. Cheng, Y. Zhang, C. Li, X. Duan, X. Fu, J. Zhang, X. Zhang, Y. Ao, Cadherin-11 cooperates with inflammatory factors to promote the migration and invasion of fibroblast-like synoviocytes in pigmented villonodular synovitis. *Theranostics* **10**, 10573–10588 (2020).
9. C. G. Gahmberg, M. Gronholm, How integrin phosphorylations regulate cell adhesion and signaling. *Trends Biochem. Sci.* **47**, 265–278 (2022).
10. F. Fagotto, A. Aslemarz, EpCAM cellular functions in adhesion and migration, and potential impact on invasion: A critical review. *Biochim. Biophys. Acta Rev. Cancer* **1874**, 188436 (2020).
11. M. L. Dustin, Integrins and their role in immune cell adhesion. *Cell* **177**, 499–501 (2019).
12. T. Momose, P. C. Amadio, M. E. Zobitz, C. Zhao, K. N. An, Effect of paratenon and repetitive motion on the gliding resistance of tendon of extrasynovial origin. *Clin. Anat.* **15**, 199–205 (2002).
13. K. Spanoudes, D. Gaspar, A. Pandit, D. I. Zeugolis, The biophysical, biochemical, and biological toolbox for tenogenic phenotype maintenance in vitro. *Trends Biotechnol.* **32**, 474–482 (2014).
14. H. Svanstrom, M. Lund, M. Melbye, B. Pasternak, Concomitant use of low-dose methotrexate and NSAIDs and the risk of serious adverse events among patients with rheumatoid arthritis. *Pharmacoepidemiol. Drug Saf.* **27**, 885–893 (2018).
15. J. H. Oh, H. J. Seo, Y. H. Lee, H. Y. Choi, H. Y. Joung, S. H. Kim, Do selective COX-2 inhibitors affect pain control and healing after arthroscopic rotator cuff repair? A preliminary study. *Am. J. Sports Med.* **46**, 679–686 (2018).
16. Y. Zhuang, W. Cui, Biomaterial-based delivery of nucleic acids for tissue regeneration. *Adv. Drug Deliv. Rev.* **176**, 113885 (2021).
17. Z. Fu, X. Zhang, X. Zhou, U. Ur-Rehman, M. Yu, H. Liang, H. Guo, X. Guo, Y. Kong, Y. Su, Y. Ye, X. Hu, W. Cheng, J. Wu, Y. Wang, Y. Gu, S. F. Lu, D. Wu, K. Zen, J. Li, C. Yan, C. Y. Zhang, X. Chen, In vivo self-assembled small RNAs as a new generation of RNAi therapeutics. *Cell Res.* **31**, 631–648 (2021).
18. D. Cesana, A. Calabria, L. Rudilosso, P. Gallina, F. Benedicenti, G. Spinozzi, G. Schiroli, A. Magnani, S. Acquati, F. Fumagalli, V. Calbi, M. Witzel, F. D. Bushman, A. Cantore, P. Genovese, C. Klein, A. Fischer, M. Cavazzana, E. Six, A. Aiuti, L. Naldini, E. Montini, Retrieval of vector integration sites from cell-free DNA. *Nat. Med.* **27**, 1458–1470 (2021).
19. H. Ruan, S. Liu, F. Li, X. Li, C. Fan, Prevention of tendon adhesions by ERK2 small interfering RNAs. *Int. J. Mol. Sci.* **14**, 4361–4371 (2013).
20. S. Liu, F. Wu, S. Gu, T. Wu, S. Chen, S. Chen, C. Wang, G. Huang, T. Jin, W. Cui, B. Sarmento, L. Deng, C. Fan, Gene silencing via PDA/ERK2-siRNA-mediated electrospun fibers for peritendinous antiadhesion. *Adv. Sci.* **6**, 1801217 (2018).
21. Y. Guo, Q. Zhu, S. Chen, Y. Li, D. Fu, D. Qiao, Y. Wang, Y. Yang, Effect of sodium hyaluronate-arboxycellulose membrane (Seprafilm®) on postoperative small bowel obstruction: A meta-analysis. *Surgery* **169**, 1333–1339 (2021).
22. D. B. Johns, G. M. Keyport, F. Hoehler, G. S. diZerega; Intergel Adhesion Prevention Study Group, Reduction of postsurgical adhesions with Intergel adhesion prevention solution: A multicenter study of safety and efficacy after conservative gynecologic surgery. *Fertil. Steril.* **76**, 595–604 (2001).
23. J. Xue, J. Xie, W. Liu, Y. Xia, Electrospun nanofibers: New concepts, materials, and applications. *Acc. Chem. Res.* **50**, 1976–1987 (2017).
24. H. M. Luu, A. Chen, I. S. Isayeva, Comparative stability of the bioresorbable ferric crosslinked hyaluronic acid adhesion prevention solutions. *J. Biomed. Mater. Res. B Appl. Biomater.* **101**, 1006–1013 (2013).
25. S. Farag, P. F. Padilla, K. A. Smith, M. L. Sprague, S. E. Zimberg, Management, prevention, and sequelae of adhesions in women undergoing laparoscopic gynecologic surgery: A systematic review. *J. Minim. Invasive Gynecol.* **25**, 1194–1216 (2018).
26. M. P. Diamond, Reduction of postoperative adhesion development. *Fertil. Steril.* **106**, 994–997.e1 (2016).
27. R. James, G. Kesturu, G. Balian, A. B. Chhabra, Tendon: Biology, biomechanics, repair, growth factors, and evolving treatment options. *J. Hand Surg. Am.* **33**, 102–112 (2008).
28. J. A. McCarron, K. A. Derwin, M. J. Bey, J. M. Polster, J. P. Schils, E. T. Ricchetti, J. P. Iannotti, Failure with continuity in rotator cuff repair "healing". *Am. J. Sports Med.* **41**, 134–141 (2013).
29. C. Liu, K. Yu, J. Bai, D. Tian, G. Liu, Experimental study of tendon sheath repair via decellularized amnion to prevent tendon adhesion. *PLOS ONE* **13**, e0205811 (2018).
30. Z. Ma, Z. Yang, Q. Gao, G. Bao, A. Valiei, F. Yang, R. Huo, C. Wang, G. Song, D. Ma, Z. H. Gao, J. Li, Bioinspired tough gel sheath for robust and versatile surface functionalization. *Sci. Adv.* **7**, eabc3012 (2021).
31. M. Benjamin, E. Kaiser, S. Milz, Structure-function relationships in tendons: A review. *J. Anat.* **212**, 211–228 (2008).
32. T. Iwanaga, M. Shikichi, H. Kitamura, H. Yanase, K. Nozawa-Inoue, Morphology and functional roles of synoviocytes in the joint. *Arch. Histol. Cytol.* **63**, 17–31 (2000).
33. S. Uchiyama, P. C. Amadio, J. Ishikawa, K. N. An, Boundary lubrication between the tendon and the pulley in the finger. *J. Bone Joint Surg. Am.* **79**, 213–218 (1997).
34. D. K. Rhee, J. Marcelino, M. Baker, Y. Gong, P. Smits, V. Lefebvre, G. D. Jay, M. Stewart, H. Wang, M. L. Warman, J. D. Carpten, The secreted glycoprotein lubricin protects cartilage surfaces and inhibits synovial cell overgrowth. *J. Clin. Invest.* **115**, 622–631 (2005).
35. Y. Wang, L. Cheng, S. Wen, S. Zhou, Z. Wang, L. Deng, H. Q. Mao, W. Cui, H. Zhang, Ice-inspired superlubricated electrospun nanofibrous membrane for preventing tissue adhesion. *Nano Lett.* **20**, 6420–6428 (2020).
36. K. A. Skipper, J. G. Mikkelsen, Delivering the goods for genome engineering and editing. *Hum. Gene Ther.* **26**, 486–497 (2015).
37. L. B. Couto, K. A. High, Viral vector-mediated RNA interference. *Curr. Opin. Pharmacol.* **10**, 534–542 (2010).
38. S. C. Lin, K. Haga, X. L. Zeng, M. K. Estes, Generation of CRISPR-Cas9-mediated genetic knockout human intestinal tissue-derived enteroid lines by lentivirus transduction and single-cell cloning. *Nat. Protoc.* **17**, 1004–1027 (2022).
39. R. Kashikar, A. K. Kotha, S. Shah, P. Famta, S. B. Singh, S. Srivastava, M. B. Chougule, Advances in nanoparticle mediated targeting of RNA binding protein for cancer. *Adv. Drug Deliv. Rev.* **185**, 114257 (2022).
40. G. Prakash, A. Shokr, N. Willemen, S. M. Bashir, S. R. Shin, S. Hassan, Microfluidic fabrication of lipid nanoparticles for the delivery of nucleic acids. *Adv. Drug Deliv. Rev.* **184**, 114197 (2022).
41. C. Shen, J. Li, Y. Zhang, Y. Li, G. Shen, J. Zhu, J. Tao, Polyethylenimine-based micro/nanoparticles as vaccine adjuvants. *Int. J. Nanomedicine* **12**, 5443–5460 (2017).
42. N. Bono, F. Ponti, D. Mantovani, G. Candiani, Non-viral in vitro gene delivery: It is now time to set the bar! *Pharmaceutics* **12**, 183 (2020).
43. S. Tommasone, F. Allabush, Y. K. Tagger, J. Norman, M. Kopf, J. H. R. Tucker, P. M. Mendes, The challenges of glycan recognition with natural and artificial receptors. *Chem. Soc. Rev.* **48**, 5488–5505 (2019).
44. F. Colombo, J. Meldolesi, L1-CAM and N-CAM: From adhesion proteins to pharmacological targets. *Trends Pharmacol. Sci.* **36**, 769–781 (2015).
45. H. L. Lu, S. S. Ren, P. P. Zhang, J. D. Guo, J. H. Li, G. N. Dong, Laser-textured surface storing a carbon dots/poly(ethylene glycol)/chitosan gel with slow-release lubrication effect. *RSC Adv.* **7**, 21600–21606 (2017).
46. S. Q. Cui, L. Yu, J. D. Ding, Semi-bald micelles and corresponding percolated micelle networks of thermogels. *Macromolecules* **51**, 6405–6420 (2018).
47. S. Q. Cui, L. Yu, J. D. Ding, Thermogelling of amphiphilic block copolymers in water: ABA type versus AB or BAB type. *Macromolecules* **52**, 3697–3715 (2019).
48. Y. P. Zhuang, X. W. Yang, Y. M. Li, Y. P. Chen, X. C. Peng, L. Yu, J. D. Ding, Sustained release strategy designed for lixisenatide delivery to synchronously treat diabetes and associated complications. *ACS Appl. Mater. Interfaces* **11**, 29604–29618 (2019).
49. L. K. Lee, K. J. Bryant, R. Bouveret, P. W. Lei, A. P. Duff, S. J. Harrop, E. P. Huang, R. P. Harvey, M. H. Gelb, P. P. Gray, P. M. Curmi, A. M. Cunningham, W. B. Church, K. F. Scott, Selective inhibition of human group IIA-secreted phospholipase A2 (hGIIA) signaling reveals arachidonic acid metabolism is associated with colocalization of hGIIA to vimentin in rheumatoid synoviocytes. *J. Biol. Chem.* **288**, 15269–15279 (2013).
50. C. D. Cai, W. Wang, J. Liang, Y. G. Li, M. K. Lu, W. G. Cui, C. Y. Fan, L. F. Deng, Y. S. Li, F. Wang, S. Liu, MMP-2 responsive unidirectional hydrogel-electrospun patch loading TGF-β1 siRNA polyplexes for peritendinous anti-adhesion. *Adv. Funct. Mater.* **31**, 2008364 (2021).
51. J. Zhou, Z. Zhang, J. Joseph, X. Zhang, B. E. Ferdows, D. N. Patel, W. Chen, G. Banfi, R. Molinaro, D. Cosco, N. Kong, N. Joshi, O. C. Farokhzad, C. Corbo, W. Tao, Biomaterials and nanomedicine for bone regeneration: Progress and future prospects. *Exp. Dermatol.* **1**, 20210011 (2021).

52. X. Zhang, L. Li, J. Ouyang, L. Zhang, J. Xue, H. Zhang, W. Tao, Electroactive electrospun nanofibers for tissue engineering. *Nano Today* **39**, 101196 (2021).
53. J. Ouyang, X. Ji, X. Zhang, C. Feng, Z. Tang, N. Kong, A. Xie, J. Wang, X. Sui, L. Deng, Y. Liu, J. Kim, Y. Cao, W. Tao, In situ sprayed NIR-responsive, analgesic black phosphorus-based gel for diabetic ulcer treatment. *Proc. Natl. Acad. Sci. U.S.A.* **117**, 28667–28677 (2020).
54. W. Chen, W. Tao, Precise control of the structure of synthetic hydrogel networks for precision medicine applications. *Matter* **5**, 18–19 (2022).
55. M. Lodyga, B. Hinz, TGF-β1 –A truly transforming growth factor in fibrosis and immunity. *Semin. Cell Dev. Biol.* **101**, 123–139 (2020).
56. M. A. Travis, D. Sheppard, TGF-β activation and function in immunity. *Annu. Rev. Immunol.* **32**, 51–82 (2014).
57. L. Cheng, Y. Wang, G. Sun, S. Wen, L. Deng, H. Zhang, W. Cui, Hydration-enhanced lubricating electrospun nanofibrous membranes prevent tissue adhesion. *Research* **2020**, 4907185 (2020).
58. Y. Xu, G. Shi, J. Tang, R. Cheng, X. Shen, Y. Gu, L. Wu, K. Xi, Y. Zhao, W. Cui, L. Chen, ECM-inspired micro/nanofibers for modulating cell function and tissue generation. *Sci. Adv.* **6**, eabc2036 (2020).
59. J. Zou, M. Lu, S. Chen, C. Cai, Z. Yao, W. Cui, C. Fan, S. Liu, Beeswax-inspired superhydrophobic electrospun membranes for peritendinous anti-adhesion. *Mater. Sci. Eng. C Mater. Biol. Appl.* **116**, 111166 (2020).

Acknowledgments
Funding: This work was supported by the National Natural Science Foundation of China (51873107),Program of Shanghai Academic/Technology Research Leader (22XD1422600), the Shanghai Municipal Education Commission–Gaofeng Clinical Medicine Grant Support (20171906), and the GuangCi Professorship Program of Ruijin Hospital Shanghai Jiao Tong University School of Medicine. **Author contributions:** L.X., J.L., and W.C. designed the lubricated gene-hydrogel patch. L.X., Z.W., and Y.Z. contributed to the synthesis of PEG polyester. L.X., L.J., and F.W. contributed to the synthesis of PEI-PBA. L.X., J.L., and F.L. contributed to the material testing and analysis. L.X., J.L., and Q.S. contributed to the animal experiments. L.X. performed all experimental data acquisition and statistical analysis. L.X., J.L., L.D., and W.C. wrote and revised the manuscript. **Competing interests:** The authors declare that they have no competing interests. **Data and materials availability:** All data needed to evaluate the conclusions in the paper are present in the paper and/or the Supplementary Materials.

Submitted 10 May 2022
Accepted 6 January 2023
Published 10 February 2023
10.1126/sciadv.adc9375